



The thermodynamics of non-equilibrium interfaces during phase transformations in concentrated multicomponent alloys

Christopher Hareland, Gildas Guillemot, Charles-André Gandin, Peter Voorhees

► To cite this version:

Christopher Hareland, Gildas Guillemot, Charles-André Gandin, Peter Voorhees. The thermodynamics of non-equilibrium interfaces during phase transformations in concentrated multicomponent alloys. *Acta Materialia*, 2022, 241, pp.118407. 10.1016/j.actamat.2022.118407 . hal-03838044

HAL Id: hal-03838044

<https://hal.science/hal-03838044>

Submitted on 3 Nov 2022

HAL is a multi-disciplinary open access archive for the deposit and dissemination of scientific research documents, whether they are published or not. The documents may come from teaching and research institutions in France or abroad, or from public or private research centers.

L'archive ouverte pluridisciplinaire **HAL**, est destinée au dépôt et à la diffusion de documents scientifiques de niveau recherche, publiés ou non, émanant des établissements d'enseignement et de recherche français ou étrangers, des laboratoires publics ou privés.

The thermodynamics of non-equilibrium interfaces during phase transformations in concentrated multicomponent alloys

Christopher A. Hareland^{a,*}, Gildas Guillemot^b, Charles-André Gandin^b, Peter W. Voorhees^a

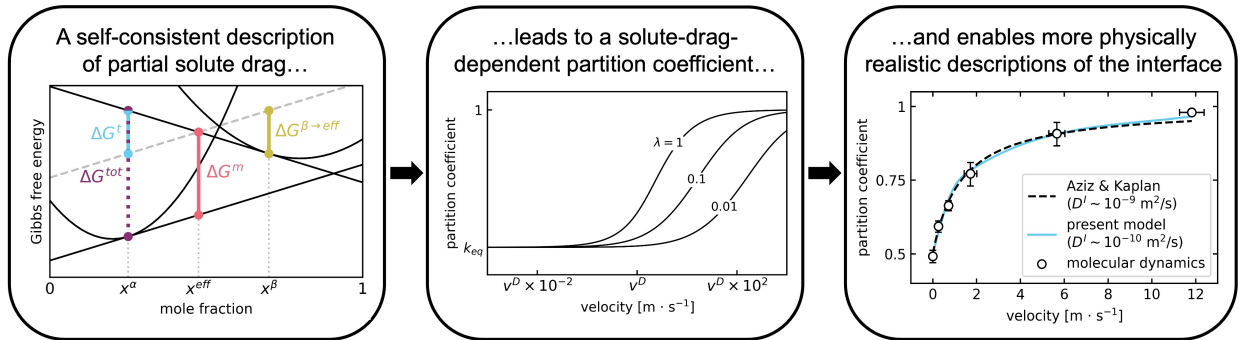
^aDepartment of Materials Science and Engineering, Northwestern University, 2220 Campus Drive, Evanston IL 60208, USA

^bMines Paris, PSL University, CEMEF UMR CNRS 7635, CS10207, 06904 Sophia Antipolis, France

Abstract

A unified thermodynamic description of moving non-equilibrium interfaces is developed for both solid/solid and solid/liquid transformations. The theory is applicable to concentrated multicomponent alloys where diffusion is possible in both phases or in just the parent phase, and where energy is dissipated due to solute drag. To be consistent with energy dissipation, we find that solute drag affects both the velocity of the interface and distribution coefficients for the compositions of the two phases at the interface. In the limit of binary alloy solidification, the theory predicts significant changes in the interfacial compositions from that given by the phase diagram at velocities commonly found during additive manufacturing. Since the distribution coefficient is affected by solute drag, the solute-trapping behavior observed in molecular dynamics simulations implies that the interfacial diffusivity lies between the diffusivity of the bulk solid and liquid. A comparison to past work on non-equilibrium interfaces during solid/solid and solid/liquid phase transformations is also given.

Graphical Abstract



Keywords: phase transformations, multicomponent alloys, modeling, thermodynamics, kinetics

*Corresponding author.

E-mail address: chris.hareland@u.northwestern.edu (C.A. Hareland)

1. Introduction

Additive manufacturing (AM) has been increasing in popularity due to the exceptional control it offers over macroscopic part geometry. The final properties of components made via AM are controlled by the solidification microstructures that form during processing. Because the solidification velocities in powder-bed fusion AM processes can easily approach $\sim 1 \text{ m} \cdot \text{s}^{-1}$ [1, 2, 3], quantitative predictions of the microstructures formed during AM require models of rapid solidification that incorporate the effects of an interface that departs from local equilibrium [4, 5]. This is further supported by observations of non-equilibrium effects such as solute trapping via experiment [6, 7], molecular dynamics simulations [8, 9], phase-field simulations [10, 11], and phase-field-crystal simulations [12].

A central assumption of many models of the conditions at interfaces during rapid solidification is negligible mass diffusion in the solid. The literature on non-equilibrium solid/solid transformations has evolved somewhat independently from that for solidification. Solid-state transformations are primarily concerned with transformations for which the rate is controlled by diffusion in both the parent (β) and growing (α) phases [13, 14, 15], while rapid solidification is able to safely neglect diffusion in the growing (solid) phase and focuses on effects such as solute trapping [16, 17, 18, 19].

Additionally, during both rapid solidification and solid/solid phase transformations, the phenomenon known as “solute drag” consumes part of the total driving force for transformation to desorb solute from the interface, which reduces the driving force available to drive the motion of the interface. Since Hillert and Sundman [20] first introduced a unified treatment of solute drag at grain boundaries and solid/liquid interfaces, the effects of solute drag have been shown to be significant through both molecular dynamics [8, 9] and phase-field simulations [10, 11, 21, 22], as well as analytical modeling of experimental results [23, 24, 25, 26, 27].

A wide variety of sharp-interface models have been developed to describe the effects of solute drag during phase transformations. *Full-drag models* — the most famous of which is the Continuous Growth Model (CGM) of Aziz [16, 17, 18] — assume that material adsorbs to the interface at the interfacial composition of the parent phase, x^β . Before the material is incorporated into the growing phase at x^α , an amount of solute equal to $x^\beta - x^\alpha$ must be desorbed from the interface back into the parent phase, which is exactly the solute-drag effect described above. In *partial-drag models*, which arose from the rapid solidification community [19], the degree of solute drag can be varied with the “solute-drag parameter”, λ , which weights the interfacial compositions of the growing and the parent phases to give an “effective concentration” of the material adsorbing to the interface:

$$x^{eff} = \lambda x^\beta + (1 - \lambda)x^\alpha \quad (1)$$

In these treatments of solidification, λ is typically assumed to vary between zero (“zero drag”) and unity (“full drag”) [19, 25], but this domain will be more rigorously defined in Section 2.2. Higher values of λ indicate increasingly favorable adsorption of solute to the interface from the growing phase and a correspondingly larger reduction in the driving force available for interface motion due to the need to desorb this extra solute. Alternatively, *partial-drag models from bulk diffusion* describe solid/solid transformations by defining the interfacial concentration, x^{tr} , in terms of the bulk fluxes in each phase [13, 14] instead of a solute-drag parameter. However, these models assume that material always adsorbs to the interface with a composition

x^β , implying that the interfacial velocity is always described by the case of complete solute drag. Thus, this *partial-drag from bulk diffusion* approach cannot treat partial solute drag during rapid solidification, which subsequent molecular dynamics simulations [8, 9] found to be important. A detailed comparison and discussion of these three approaches (*full-drag*, *partial-drag* and *partial-drag from bulk diffusion*) is found in Section 4. Regardless, assigning a representative concentration to a sharp interface enables more detailed and physically realistic sharp-interface models.

Additionally, many of the models for non-equilibrium interfaces are limited to binary alloys. Since most alloys used commercially contain appreciable amounts of several solutes, a model that allows for many components and non-dilute solutions is needed. Sharp-interface models have been developed for multicomponent systems by, for example, Ludwig [28] for solidification under the no-drag case of the CGM [18], Sobolev et al. [29] for solute partitioning considering local non-equilibrium diffusion in the liquid, Kuang et al. [30] for a two-step drag model under the thermodynamic extremal principle, Wang et al. [31] for full-drag models under local non-equilibrium diffusion and the thermodynamic extremal principle, and Du et al. for the CGM with drag during rapid solidification [32] and solid-state transformations [33]. Additionally, Du et al. [32] formulated a model for multicomponent alloys that can be coupled with CALPHAD methodology. However, a complete model including partial solute drag and diffusion in both phases for multicomponent alloys is not available. Herein, we develop a model for multicomponent alloys incorporating both bulk diffusion and partial solute drag at interfaces, employing the general approach to non-equilibrium migrating interfaces developed for binary alloys by Gurtin and Voorhees [34].

Due to the various definitions of the interfacial concentration, sharp-interface models differ in their selection and development of the kinetic equations describing two energy-dissipating processes: interface migration and trans-interface diffusion [35]. The relationships between the driving forces, which are functions of the jumps across the interface in both the grand potential and the diffusion potentials, and the interfacial fluxes for each process are described by kinetic equations known as “interfacial response functions”. There are two types of interfacial response function; the velocity response function (VRF) gives the interface velocity in the direction normal to the interface, v ($\text{m} \cdot \text{s}^{-1}$), and the concentration response functions (CRFs) can be used to determine the ratio of the concentrations of each component i in each phase at the interface, i.e., the velocity-dependent distribution coefficient, which is defined as $k_v^i = x_i^\alpha / x_i^\beta$ for the growth of α from β . Note that a binary alloy will have one VRF and one CRF, while an N -component alloy will have one VRF and $N - 1$ CRFs (one for each independent chemical species, $i \in \{2, \dots, N\}$). For binary alloys, the fluxes for these processes can be obtained from an interdiffusion approach and the driving forces can be obtained from graphical constructions [15, 35]. These graphical constructions are described in Section 4 to illustrate various interpretations of these fluxes and driving forces. For multicomponent alloys, a dissipation relation [36, 37, 38] combined with an interfacial mass balance is a convenient method of obtaining the fluxes and driving forces in a self-consistent way.

To predict the interface response functions during both rapid solidification and solid-state transformations, a model for phase transformations in concentrated multicomponent alloys under general non-equilibrium conditions at the interface is required. Here, we unify the approaches developed for non-equilibrium interfaces in the solidification and solid-state communities by allowing diffusion in the growing phase, but retaining the effective concentration defined in Eq. (1) to incorporate partial solute drag at the

velocities relevant to additive manufacturing. The effects of solid-state diffusion and partial solute drag are incorporated self-consistently into the interfacial response functions for multicomponent alloys using an energy dissipation approach [34], which also allows for additional effects, such as interfacial energy, to be incorporated if desired.

2. Non-equilibrium Thermodynamics of Interface Migration

2.1. Interfacial mass balance

For an N -component system with a curved interface, Gurtin and Voorhees [34] give a mass balance for component i in phase ϕ with respect to a control volume attached to an interface moving with velocity \mathbf{v} ($\text{m} \cdot \text{s}^{-1}$). Throughout this work, it is assumed that the partial molar volumes, V_i^ϕ ($\text{m}^3 \cdot \text{mol}^{-1}$), of all i components in each phase are equal to the molar volume of the alloy, $V_m = \sum_{i=1}^N V_i^\phi x_i^\phi$ ($\text{m}^3 \cdot \text{mol}^{-1}$), where x_i^ϕ ($\text{mol} \cdot \text{mol}^{-1}$) is the mole fraction of component i in phase ϕ . Because $\sum_{i=1}^N x_i^\phi = 1$, this is equivalent to a constant number density, $\rho_i^\phi = 1/V_i^\phi$ ($\text{mol} \cdot \text{m}^{-3}$), for all i components in each phase, i.e., $\rho_i^\phi = \rho_0$. Additionally, atoms are assumed to diffuse by a direct exchange mechanism—neglecting sources, sinks, and diffusion of vacancies—so there are $N - 1$ independent fluxes in an N -component system, denoted by the subscript $i \in \{2, \dots, N\}$. In the absence of surface diffusion, the mass balance for component i at the interface in phase ϕ is given by

$$\dot{j}_i^\phi + \rho_0 x_i^{eff} \mathbf{v} \cdot \hat{\mathbf{n}}^\phi = -\mathbf{J}_i^\phi \cdot \hat{\mathbf{n}}^\phi + \rho_0 x_i^\phi \mathbf{v} \cdot \hat{\mathbf{n}}^\phi \quad (2)$$

where \dot{j}_i^ϕ ($\text{mol} \cdot \text{m}^{-2} \cdot \text{s}^{-1}$) is the diffusion flux entering phase ϕ through the interface, $\rho_0 x_i^\phi$ ($\text{mol} \cdot \text{m}^{-3}$) is the volumetric concentration of component i in phase ϕ at the interface, $\rho_0 x_i^{eff}$ ($\text{mol} \cdot \text{m}^{-3}$) is the effective volumetric concentration of component i within the interface as defined by Eq. (1), and \mathbf{J}_i^ϕ ($\text{mol} \cdot \text{m}^{-2} \cdot \text{s}^{-1}$) and $\hat{\mathbf{n}}^\phi$ are the bulk flux of component i in phase ϕ and the outward normal vector of phase ϕ , respectively.

To describe the growth of α from β , we assume that the growing and parent phases remain in continuous contact (i.e., $\hat{\mathbf{n}}^\alpha = -\hat{\mathbf{n}}^\beta$ and $\mathbf{v} \cdot \hat{\mathbf{n}}^\alpha = -\mathbf{v} \cdot \hat{\mathbf{n}}^\beta = v$) and define the bulk flux in each phase at the interface as $J_i^\phi = \mathbf{J}_i^\phi \cdot \hat{\mathbf{n}}^\alpha$. Under these assumptions, Eq. (2) gives two expressions for the trans-interface diffusive flux of component i , J_i^t , where $J_i^t = j_i^\beta = -j_i^\alpha$:

$$J_i^t = \rho_0 v (x_i^{eff} - x_i^\alpha) + J_i^\alpha \quad (3)$$

$$J_i^t = \rho_0 v (x_i^{eff} - x_i^\beta) + J_i^\beta \quad (4)$$

The terms comprising Eqs. (3) and (4) are shown in Figure 1, where a closed system is schematized by a domain Ω comprised of N components in two bulk phases, α and β , which occupy the regions Ω^α and Ω^β , respectively. The system is surrounded by an inert medium, which enforces zero-flux boundary conditions everywhere except at the surface $\partial\Omega$, which is the interface between Ω^α and Ω^β . J_i^t is the flux of component i rejected from the interface back into the parent phase, which is the flux giving rise to the solute-drag effect. The first terms on the right-hand sides of Eqs. (3) and (4) result solely from the motion of the interface, and the second terms on the right-hand sides are the bulk diffusion fluxes evaluated at the interface. Equating Eqs. (3) and (4) gives the standard interfacial mass balance:

$$[J_i] = \rho_0 v [x_i] \quad (5)$$

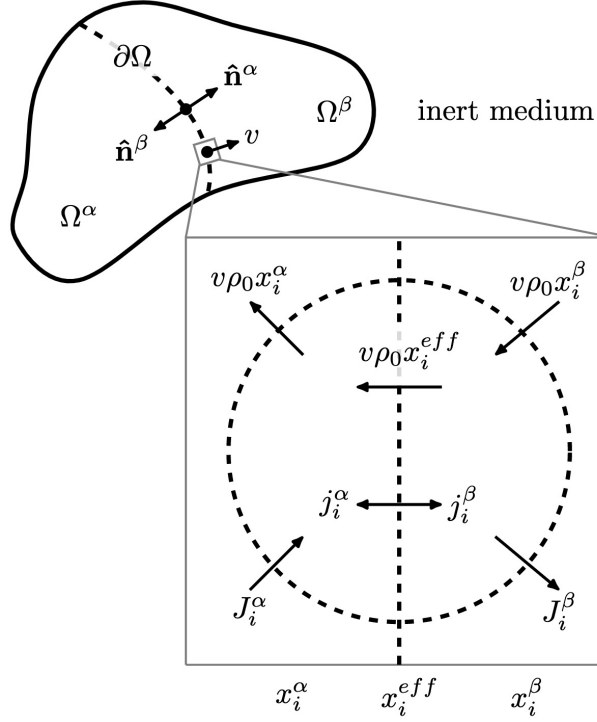


Figure 1: Schematic of a system with a sharp interface comprised of the growing (α) and parent (β) phase surrounded by an inert medium. The inset shows an interfacial control volume in each phase. The terms comprising the fluxes defined in Eqs. (2) – (4) are marked, and the inset illustrated is sufficiently small for each flux component to be normal to the interface.

where the notation $[\![\Phi]\!] = \Phi^\beta - \Phi^\alpha$ denotes the jump across the interface in a quantity Φ . Recovering the standard mass-balance condition indicates that the net mass transfer for the phase transformation is independent of the interfacial concentration and the effects of partial solute drag.

2.2. Energy dissipation

The thermodynamics of interfaces in this non-equilibrium case must be consistent with the first and second laws of thermodynamics. In general, evolution equations are obtained from the rate of entropy production; however, if the system is assumed to be at constant temperature and volume, this is equivalent to the rate of Helmholtz energy dissipation. Because the phenomenological equations for multicomponent systems can require many kinetic coefficients, the thermodynamic extremal principle has been widely used to formulate the evolution equations of multicomponent systems [30, 31, 39]. Here, we instead use the classical dissipation approach [36, 37, 38], which requires that the Helmholtz free energy decreases, but not necessarily at the maximum possible rate. Using the principle that the energy must decrease, it is possible to identify constitutive laws for non-equilibrium interfaces [34, 40, 41, 42].

The dissipation rate of Helmholtz free energy \dot{F} ($\text{J} \cdot \text{s}^{-1}$) for this system with a planar interface is

$$\dot{F} = \int_{\Omega^\alpha} \frac{\partial f_v^\alpha}{\partial t} dV + \int_{\Omega^\beta} \frac{\partial f_v^\beta}{\partial t} dV - \int_{\partial\Omega} \llbracket f_v \rrbracket v dA \quad (6)$$

144 where $f_v^\phi = \rho_0 \sum_{i=1}^N \mu_i^\phi x_i^\phi$ ($\text{J} \cdot \text{m}^{-3}$) is the volumetric Helmholtz free energy in phase ϕ at constant temper-
 145 ature and volume. Each volume integral describes the energy dissipation rate in a bulk phase, while the
 146 surface integral describes the energy dissipation rate due to creation of α lattice sites at the expense of β
 147 lattice sites resulting from the motion of the interface. For a closed, isothermal, stress-free system, we have

$$\frac{\partial f_v^\phi}{\partial t} = \rho_0 \sum_{i=2}^N \tilde{\mu}_i^\phi \frac{\partial x_i^\phi}{\partial t} \quad (7)$$

148 where $\rho_0 \tilde{\mu}_i^\phi = \rho_0 (\mu_i^\phi - \mu_1^\phi) = \partial f_v^\phi / \partial x_i$ ($\text{J} \cdot \text{m}^{-3}$) is the diffusion potential of component i with respect to the
 149 $i = 1$ component. Additionally, the standard continuity equation without sources or sinks of mass is given
 150 by

$$\rho_0 \frac{\partial x_i^\phi}{\partial t} = -\nabla \cdot \mathbf{J}_i^\phi \quad (8)$$

151 By substituting Eqs. (7) and (8) into Eq. (6) and then using the product rule for divergences followed by
 152 the divergence theorem, the fluxes and driving forces comprising \dot{F} can be split into terms describing the
 153 dissipation by diffusion in the bulk, \dot{F}_Ω , and by processes occurring at the interface, $\dot{F}_{\partial\Omega}$:

$$\dot{F}_\Omega = \int_{\Omega^\alpha} \sum_{i=2}^N \nabla \tilde{\mu}_i^\alpha \cdot \mathbf{J}_i^\alpha dV + \int_{\Omega^\beta} \sum_{i=2}^N \nabla \tilde{\mu}_i^\beta \cdot \mathbf{J}_i^\beta dV \quad (9)$$

$$\dot{F}_{\partial\Omega} = - \int_{\partial\Omega} \left\{ \sum_{i=2}^N \tilde{\mu}_i^\alpha \mathbf{J}_i^\alpha \cdot \hat{\mathbf{n}}^\alpha + \sum_{i=2}^N \tilde{\mu}_i^\beta \mathbf{J}_i^\beta \cdot \hat{\mathbf{n}}^\beta + \llbracket f_v \rrbracket v \right\} dA \quad (10)$$

154 The total free energy dissipation, $\dot{F} = \dot{F}_\Omega + \dot{F}_{\partial\Omega}$, is equivalent to Eq. (8) of Ref. [31] if the assumption of
 155 local equilibrium holds for mass transfer in the bulk phases. Inserting the mass-balances, Eqs. (3) and (4),
 156 into Eq. (10) and rearranging gives

$$\dot{F}_{\partial\Omega} = \int_{\partial\Omega} \left\{ - \left(\llbracket \Omega_v \rrbracket + \rho_0 \sum_{k=2}^N x_k^{eff} \llbracket \tilde{\mu}_k \rrbracket \right) v + \sum_{i=2}^N \llbracket \tilde{\mu}_i \rrbracket J_i^t \right\} dA \quad (11)$$

157 where Ω_v^ϕ ($\text{J} \cdot \text{m}^{-3}$) is the volumetric grand potential in phase ϕ :

$$\Omega_v^\phi = f_v^\phi(x_2^\phi, \dots, x_N^\phi) - \rho_0 \sum_{i=2}^N \tilde{\mu}_i^\phi x_i^\phi \quad (12)$$

158 Using the Helmholtz free energy as defined previously in the case of constant temperature and volume, the
 159 molar grand potential reduces to the chemical potential of the dependent component, i.e., $\rho_0^{-1} \Omega_v^\phi = \mu_1^\phi$, as
 160 noted by Chatterjee and Moelans [43]. The first term of Eq. (11) describes the dissipation due to the motion
 161 of the interface that involves the adsorption of components at their respective effective concentrations, x_i^{eff} ,
 162 while the second term describes the dissipation due to solute drag that requires the desorption of excess
 163 solute, i.e., the concentration above that of the growing phase x_i^α , from the interface back into the parent
 164 phase.

165 For \dot{F} to be strictly negative for any process, we require that both \dot{F}_Ω and $\dot{F}_{\partial\Omega}$ be negative. Requiring
 166 $\dot{F}_\Omega < 0$ can lead to the usual relationship between the mass flux and the gradient in diffusion potential,

167 which is discussed further in Section 2.4. To guarantee that $\dot{F}_{\partial\Omega} < 0$ in the most general case, each term in
 168 Eq. (11) must be negative. This gives two dissipation inequalities:

$$v \left(\llbracket \Omega_v \rrbracket + \rho_0 \sum_{k=2}^N x_k^{eff} \llbracket \tilde{\mu}_k \rrbracket \right) > 0 \quad (13)$$

$$\sum_{i=2}^N \llbracket \tilde{\mu}_i \rrbracket J_i^t < 0 \quad (14)$$

169 Because the solute-drag parameter, λ , appears in both Eqs. (13) and (14) through x^{eff} , these dissipation
 170 inequalities provide upper and lower bounds on the solute-drag parameter for the $\beta \rightarrow \alpha$ transformation
 171 considered here. The lower bound of λ is set by Eq. (14) which, because $\llbracket \tilde{\mu}_i \rrbracket$ is independent of x_i^{eff} , entirely
 172 depends on the trans-interface diffusion flux that gives rise to solute drag, J_i^t , defined in Eqs. (3) and (4).
 173 Physically, for the product $\llbracket \tilde{\mu}_i \rrbracket J_i^t$ to be negative, the effective concentration must be sufficiently high such
 174 that the magnitude of the flux due to the motion of the interface, $\rho_0 v (x_i^{eff} - x_i^\alpha)$, exceeds the magnitude
 175 of the flux due to bulk diffusion, J_i^α . For example, if $J_i^\alpha = 0$, as is typically assumed in rapid solidification
 176 ($\alpha = s$, $\beta = l$), we must have $x_i^{eff} > x_i^s$, i.e., $\lambda > 0$ (assuming $\llbracket \tilde{\mu}_i \rrbracket < 0$ and $x_i^l > x_i^s$). The upper bound of
 177 λ is set by Eq. (13), as the $\beta \rightarrow \alpha$ transformation requires $v > 0$ by definition. While the upper bound was
 178 assumed to be unity in the solidification models in which λ was first introduced [18, 19], the upper bound
 179 from Eq. (13) can be greater than one, and corresponds to a system for which the term in the parenthesis
 180 is zero, which occurs when the effects of solute drag are sufficiently large to completely halt the motion of
 181 the interface.

182 Additionally, we note that there is only a single value of λ in the current formulation, even for multi-
 183 component systems. From the definition of x_i^{eff} in Eq. (1), it can be shown that the value of λ must be
 184 the same for all $i \in \{1, \dots, N\}$ components in order for $\sum_{i=1}^N x_i^{eff} = 1$. As such, λ represents the response
 185 of the interface to the collective effect of solute drag from all components. However, if one species interacts
 186 much more strongly with the interface than the others, λ could become a function of x_i^{eff} .

187 2.3. Interfacial response functions

188 Assuming that the two types of dissipative processes obey linear kinetics gives the interfacial response
 189 functions from Eqs. (13) and (14), a VRF and $N - 1$ CRFs, respectively:

$$v = M^m \rho_0^{-1} \left(\llbracket \Omega_v \rrbracket + \rho_0 \sum_{k=2}^N x_k^{eff} \llbracket \tilde{\mu}_k \rrbracket \right) - \sum_{j=2}^N m_j^m \llbracket \tilde{\mu}_j \rrbracket \quad (15)$$

$$J_i^t = m_i^t \left(\llbracket \Omega_v \rrbracket + \rho_0 \sum_{k=2}^N x_k^{eff} \llbracket \tilde{\mu}_k \rrbracket \right) - \rho_0 \sum_{j=2}^N M_{ij}^t \llbracket \tilde{\mu}_j \rrbracket \quad (16)$$

190 where M^m , m_j^m , m_i^t , and M_{ij}^t ($\text{mol} \cdot \text{m} \cdot \text{J}^{-1} \cdot \text{s}^{-1}$) are the kinetic coefficients. The processes of interface
 191 migration and trans-interface diffusion are denoted with superscript m and t , respectively. The coefficients
 192 M^m and M_{ij}^t represent the mobility of the interface and the mobility of component i across the interface,
 193 respectively, and the coefficients m_j^m and m_i^t represent the cross-coupling between the processes of interface

194 migration and trans-interface diffusion. These constitutive equations at the interface can be written in
 195 matrix-vector form as:

$$\begin{bmatrix} \rho_0 v \\ J_2^t \\ \vdots \\ J_N^t \end{bmatrix} = \rho_0 \begin{bmatrix} M^m & m_2^m & \cdots & m_N^m \\ m_2^t & M_{22}^t & \cdots & M_{2N}^t \\ \vdots & \vdots & \ddots & \vdots \\ m_N^t & M_{N2}^t & \cdots & M_{NN}^t \end{bmatrix} \begin{bmatrix} \rho_0^{-1} \left(\llbracket \Omega_v \rrbracket + \rho_0 \sum_{k=2}^N x_k^{eff} \llbracket \tilde{\mu}_k \rrbracket \right) \\ -\llbracket \tilde{\mu}_2 \rrbracket \\ \vdots \\ -\llbracket \tilde{\mu}_N \rrbracket \end{bmatrix} \quad (17)$$

196 where the matrix of kinetic coefficients must be positive-definite. Note that when moving from Eq. (15) to
 197 Eq. (17), a factor of ρ_0 was multiplied into Eq. (15) in order to write the left-hand side of the VRF as a
 198 flux. This result only assumes that energy must decrease during isothermal processes, and no assumption
 199 has been made regarding the rate of energy dissipation. Thus, it is not surprising that Eq. (17) differs from
 200 the result obtained by maximizing the energy dissipation [31].

201 Hereafter, we neglect cross-coupling between the fluxes and driving forces for the two types of interfacial
 202 processes by letting $m_i^m = m_i^t = 0$, which reduces Eqs. (15) and (16) to:

$$v = M^m \rho_0^{-1} \left(\llbracket \Omega_v \rrbracket + \rho_0 \sum_{k=2}^N x_k^{eff} \llbracket \tilde{\mu}_k \rrbracket \right) \quad (18)$$

$$J_i^t = -\rho_0 \sum_{j=2}^N M_{ij}^t \llbracket \tilde{\mu}_j \rrbracket \quad (19)$$

203 2.4. Kinetic coefficients

204 The M^m kinetic coefficient describes the mobility of the interface, and is typically given by

$$M^m = \frac{v_0}{RT} \quad (20)$$

205 where v_0 ($\text{m} \cdot \text{s}^{-1}$) is a constitutive parameter representing the maximum possible transformation velocity
 206 and T (K) is the interfacial temperature [18, 31, 33]. The value of v_0 for a specific material system must be
 207 determined experimentally. For solidification processes, v_0 is typically found to be on the order of, but less
 208 than, the velocity of sound in the liquid, $\sim 10^3 \text{ m} \cdot \text{s}^{-1}$. With this kinetic coefficient, the VRF in Eq. (18)
 209 contains two constitutive parameters: v_0 and λ .

210 From Eq. (9), assuming linear kinetics between the mass flux and gradient in diffusion potential yields
 211 the usual relationship between the mass flux and the gradient in diffusion potential for a multicomponent
 212 alloy:

$$\mathbf{J}_i^\phi = -\rho_0 \sum_{j=2}^N M_{ij}^\phi \nabla \tilde{\mu}_j^\phi \quad (21)$$

213 where the kinetic coefficients M_{ij}^ϕ ($\text{mol} \cdot \text{m}^2 \cdot \text{J}^{-1} \cdot \text{s}^{-1}$) describe diffusion in the bulk phase ϕ . Following
 214 Andersson and Ågren [44] under the assumption of constant molar volumes, the M_{ij}^ϕ coefficients are given
 215 by:

$$M_{ij}^\phi = \sum_{k=1}^N (\delta_{ik} - x_i) (\delta_{jk} - x_j) x_k \frac{D_k^*}{RT} \quad (22)$$

where D_k^* is the tracer diffusivity of component k . To convert from the bulk M_{ij}^ϕ kinetic coefficients, which link fluxes to gradients in diffusion potential, to the M_{ij}^t coefficients of the present sharp-interface model, which link fluxes to jumps in diffusion potentials, we write

$$M_{ij}^t = M_{ij}^\phi / \delta \quad (23)$$

where δ is approximately the width of the interface. Additionally, because the M_{ij}^t coefficients describe the motion of solute across the interface, we take the concentrations as the effective concentrations. Finally, we assume that $D_k^* = D_i^I$, where D_i^I is the diffusivity of component i within the interface. These assumptions yield the following M_{ij}^t kinetic coefficients:

$$M_{ij}^t = -x_i^{eff} x_j^{eff} \frac{v_i^D}{RT}, \quad i \neq j \quad (24)$$

$$M_{ii}^t = x_i^{eff} (1 - x_i^{eff}) \frac{v_i^D}{RT}, \quad i = j \quad (25)$$

where we have introduced the trans-interface diffusive speed, $v_i^D = D_i^I / \delta$, which describes the velocity at which an atom of component i traverses the interface. As both D_i^I and δ are typically unknown, v_i^D is often used alongside v_0 to apply the interfacial response functions to experimental or simulation data. With these kinetic coefficients, each CRF in Eq. (19) (i.e., one for the trans-interface diffusion of each component $i \in \{2, \dots, N\}$) contains two constitutive parameters: λ and v_i^D . Notably, the solute-drag parameter, λ , appears in both interfacial response functions, self-consistently incorporating the effects of partial solute drag as an additional degree of freedom available to describe the transformation.

These kinetic coefficients can be modified accordingly by following Refs. [45, 44], if, for example, vacancy diffusion cannot be neglected, the assumption of constant molar volumes for all components is poor, or interstitial species are to be considered.

2.5. Incorporating additional effects

The effects of interfacial energy can be incorporated into the dissipation relation (see, for example, Ramanathan and Voorhees [42]) via an additional term in Eq. (10):

$$\dot{F}_\kappa = \int_{\partial\Omega} \gamma \kappa v \, dA \quad (26)$$

where γ ($\text{J} \cdot \text{m}^{-2}$) is the interfacial energy and $\kappa = \nabla \cdot \hat{\mathbf{n}}^\alpha$ (m^{-1}) is the interfacial mean curvature of the growing phase. Eq. (26) assumes a constant, isotropic surface energy, but anisotropy can be added if desired. Carrying this extra term through the dissipation relation, the CRF in Eq. (19) is unchanged, but the VRF in Eq. (18) becomes

$$v = M^m \rho_0^{-1} \left(\llbracket \Omega_v \rrbracket + \rho_0 \sum_{k=2}^N x_k^{eff} \llbracket \tilde{\mu}_k \rrbracket - \gamma \kappa \right) \quad (27)$$

assuming $\gamma \kappa$ is sufficiently small such that the driving force does not change sign. The presence of an interfacial energy reduces the driving force for interfacial motion, but does not change the driving force for diffusion through the interface.

Additionally, due to the use of the dissipation relation, it is straightforward to include additional terms describing the energy dissipation due to, for example, local non-equilibrium diffusion [27, 31], elastic stress [40, 41], or convection in the melt (as proposed by [46]), and the interfacial response functions will follow naturally.

2.6. The case of a stationary interface

Thus far, the analysis has not made any assumptions about diffusion in the growing phase. Inserting Eq. (3) into Eq. (19) gives the following CRF:

$$\rho_0 v \left(x_i^{eff} - x_i^\alpha \right) + J_i^\alpha = -\rho_0 \sum_{j=2}^N M_{ij}^t \llbracket \tilde{\mu}_j \rrbracket \quad (28)$$

In the $v = 0$ limit, which could be relevant in certain solid/solid transformations where the mobility of the interface, M^m , is exceptionally low, only J_i^α remains on the left-hand side of Eq. (28). Because it is assumed that α and β are in continuous contact and no surface diffusion is occurring, the $v = 0$ limit also gives $J_i^\alpha = J_i^\beta$ from Eq. (5), reducing Eq. (28) to

$$J_i^\alpha = J_i^\beta = -\rho_0 \sum_{j=2}^N M_{ij}^t \llbracket \tilde{\mu}_j \rrbracket \quad (29)$$

which states that there can still be fluxes across a stationary interface if the diffusion potentials across the interface are unequal, and that the fluxes at the interface will be equal in both phases. Thus, even in the absence of interfacial motion, the interfacial compositions are functions of the fluxes flowing through the interface. Eq. (29) can be viewed as the mass-transfer analog of the thermal boundary resistance [47] — also known as the Kapitza resistance, where the magnitude of the thermal flux, J_Q , across an interface is given by $J_Q = M_Q \llbracket T \rrbracket$ — and has been observed in the sharp-interface limit of diffuse-interface theories for diffusion couples [48].

3. Solidification of binary alloys

To illustrate the physics described by this model and the effect of the solute-drag parameter, Eqs. (18) and (19) are applied to the solidification ($\alpha = s$, $\beta = l$) of a binary alloy (components a and b) with a planar interface and zero diffusion in the solid. Because the diffusive speed in the liquid is several orders of magnitude larger than that in the solid, this is a reasonable assumption during rapid solidification. Thus, we set $J_b^s = 0$ in Eq. (3). Under these assumptions and with the kinetic coefficients in Eqs. (20) and (25), the interfacial response functions in Eqs. (18) and (19) become

$$v = \frac{v_0}{RT} \left(x_b^{eff} \llbracket \mu_b \rrbracket + \left(1 - x_b^{eff} \right) \llbracket \mu_a \rrbracket \right) \quad (30)$$

$$\left(x_b^{eff} - x_b^s \right) v = \left(1 - x_b^{eff} \right) x_b^{eff} \frac{v^D}{RT} \left(\llbracket \mu_a \rrbracket - \llbracket \mu_b \rrbracket \right) \quad (31)$$

The full derivation of Eqs. (30) and (31) from Eqs. (18) and (19), respectively, is provided in Appendix A. Note that, because of the assumption of diffusion via a direct exchange mechanism, a binary alloy only has one unique diffusive speed.

Notably, Eqs. (30) and (31) are both dependent on the degree of solute drag in the system through x_b^{eff} . Thus, λ is critical in setting both the velocity of the interface and the distribution coefficient, which follows from Eq. (31). To illustrate the effects of solute drag on the distribution coefficient, we examine a dilute-ideal solution, in which the chemical potential of component i is given by $\mu_i = \mu_i^o + RT \ln x_i$, so the driving force in Eq. (31) is

$$[\mu_a] - [\mu_b] = \mu_a^{o,l} - \mu_a^{o,s} - \mu_b^{o,l} + \mu_b^{o,s} + RT \ln \left\{ \frac{(1 - x_b^l)x_b^s}{(1 - x_b^s)x_b^l} \right\} \quad (32)$$

From the equilibrium condition, i.e., $\mu_i^l = \mu_i^s$, we have

$$\mu_i^{o,l} - \mu_i^{o,s} = RT \ln \left\{ \frac{x_i^{s,eq}}{x_i^{l,eq}} \right\} \quad (33)$$

Using the definition of x_b^{eff} and the dilute-solution approximation, i.e., $x_a^s \approx 1$ and $x_a^l \approx 1$, Eq. (31) becomes

$$(1 - k_v)\lambda v = v^D [\lambda + (1 - \lambda)k_v] \ln \left\{ \frac{k_v}{k_{eq}} \right\} \quad (34)$$

Fixing $k_{eq} = 0.25$, we solve Eq. (34) for k_v , which is plotted as a function of velocity for various values of v^D and λ . Figure 2b also provides a comparison to the CGM, shown as the dotted line. In the dilute-solution limit, the expression for the distribution coefficient from the CGM is

$$k_v = \frac{k_{eq} + v/v^D}{1 + v/v^D} \quad (35)$$

An analogous analytic expression can be obtained from the present model. Assuming an expression for k_v of a similar form to the CGM, substituting it into Eq. (34), and performing a Taylor expansion in the limit of $v \ll v^D$ yields

$$k_v = \frac{k_{eq} + \alpha v/v^D}{1 + \alpha v/v^D} \quad \text{where} \quad \alpha = \frac{k_{eq} \lambda}{k_{eq}(1 - \lambda) + \lambda} \quad (36)$$

As shown by the dotted lines in Figure 2, this expression gives a reasonable approximation to the numerical solution for k_v using Eq. (34), especially for $v < v^D$.

We employ numerical solutions to the non-linear equations in the subsequent analyses (Sections 3.1 and 3.2) and use the CRF given in Eq. (31). Note that the derivation of Eq. (35) does not incorporate λ in the solute-drag flux [18], which results in an expression for k_v that is independent of λ . The effects of this assumption on the full expression for k_v will be discussed in Section 3.2. Here, λ is present in Eq. (3), leading to a solute-drag-dependent distribution coefficient.

Because of the assumed linearity between the fluxes and gradients in diffusion potentials, the k_v curve obtained here resembles that of the CGM; it is a sigmoidal curve with the asymptotic behavior $k_v \rightarrow k_{eq}$ as $v \rightarrow 0$ and $k_v \rightarrow 1$ (i.e., “complete solute trapping”) as $v \rightarrow \infty$. However, the model does not include potentially important effects that occur in the very high velocity regime; see, for example, Sobolev [49, 50], Li et al. [25], and Wang et al. [27, 31, 51]. These models show a sharp transition to complete solute trapping when v reaches the bulk diffusion speed in the liquid, which is typically $\approx 10 \text{ m} \cdot \text{s}^{-1}$. Thus, our model only gives approximate values of the velocities in this range, and is most relevant to velocities at which only the interface departs from local equilibrium, such as those encountered in additive manufacturing. As

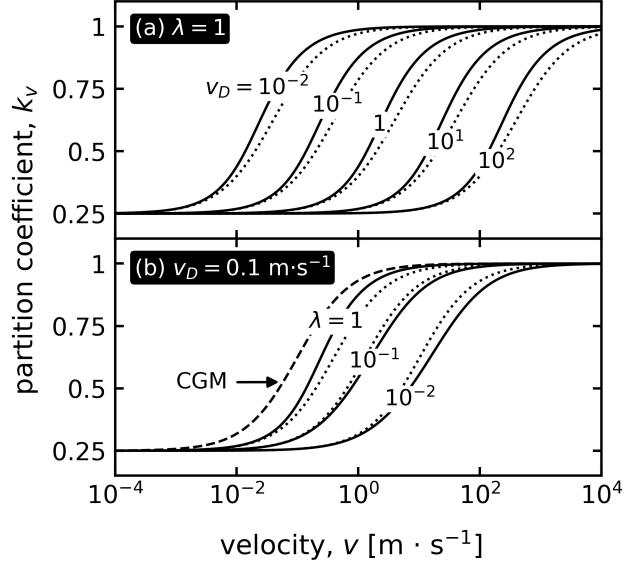


Figure 2: The velocity-dependent distribution coefficient, $k_v = x_b^s/x_b^l$, for different values of (a) the diffusive speed, v^D , and (b) the solute-drag parameter, λ . The solid curves are the numerical solution to Eq. (34), and the dotted curves are the analytical approximation in Eq. (36). Figure (b) includes (dashed line) the Aziz CGM. Increasing v^D simply translates the sigmoidal k_v curve to higher v , while decreasing λ both translates it to higher v and slightly flattens it.

can be seen from Figure 2a, increasing v^D increases the velocity at which solute trapping begins by simply translating the k_v curve along the v -axis. This is expected, as the speed at which the interface must move to trap the atom in the growing phase increases as the speed at which the atom can cross the interface, v^D , increases. Figure 2b shows that decreasing the amount of solute drag (i.e., decreasing λ) also translates the k_v curve to higher velocities. This occurs because smaller values of λ indicate that material adsorbs to the interface at a composition closer to x_b^s . Thus, less trans-interface diffusion is required to adjust x_b^{eff} to x_b^s , so x_b^s can be maintained to higher velocities than if the material adsorbs to the interface with a composition closer to x_b^l . If experimental or simulation data are available, it is possible to determine the materials parameters v_0 and λ that appear in the VRF, as shown in Section 3.1 and 3.2.

3.1. Estimation of the trans-interface diffusion coefficient

The effects of partial solute drag on the velocity of the interface can be investigated using molecular dynamics following the methodology of Yang et al. [8]. Using the tabulated velocities and Gibbs free energy differences from Table IV of the supplementary information of Ref. [8], the value of λ is determined by varying λ until the best linear-least-squares fit is obtained between the MD data and the VRF. The results are shown in Figure 3 alongside the zero-drag case. In agreement with Yang et al. [8] we find that partial solute drag is necessary to obtain a linear relationship between the measurements of the velocity and the driving force for interface motion, and that the effects of solute drag are most significant at low velocities where appreciable solute partitioning occurs and least significant at high velocities where the system approaches complete solute trapping.

From the above analysis, we obtain $v_0 = 890 \text{ m} \cdot \text{s}^{-1}$ and $\lambda = 0.29$ for the $\{100\}$ interface and $v_0 =$

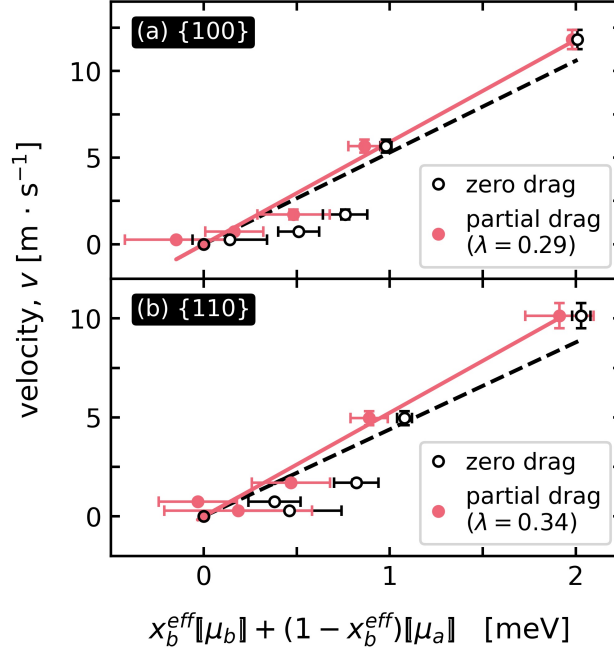


Figure 3: Fitting the driving force for interface migration to the velocity response function, Eq. (30), for (a) $\{100\}$ and (b) $\{110\}$ interfaces. Open circles are the results from the molecular dynamics simulations of Ni-Cu by Yang et al. [8].

790 $\text{m} \cdot \text{s}^{-1}$ and $\lambda = 0.34$ for the $\{110\}$ interface. These values of λ agree with the values permitted by the
 320 dissipation relation in Section 2.2, within the uncertainties in the measurements of the free energy changes
 321 from molecular dynamics. The value of T is assumed to remain constant at 1750 K. As the sound velocity
 322 in liquid Ni at 1750 K and atmospheric pressure is approximately $4000 \text{ m} \cdot \text{s}^{-1}$ [52], these values of v_0 are
 323 a factor of 5 smaller than the sound velocity.

324 The supplementary information of Ref. [8] also reports x_b^s and x_b^l at the various solidification velocities,
 325 allowing k_v to be calculated. While Yang et al. describe the k_v measurements with the CGM, i.e., Eq. (35),
 326 we use the present CRF with the reported x_b^l in Eq. (31), solving for x_b^s while determining the optimal value
 327 of v^D . Because the value of λ is already known from analyzing the velocity/driving force measurements, v^D
 328 is the only as-yet-unknown constitutive parameter in both models. Figure 4 shows the descriptions of the
 329 k_v data with both the present CRF and the CGM. Note that the current model is not able to be evaluated
 330 between the provided data points because free energies are only available at the measured velocities, so a
 331 spline was used to obtain continuous curves in both Figures 4a and 4b. The CRF gives diffusive speeds of
 332 $v^D = 0.32 \text{ m} \cdot \text{s}^{-1}$ for the $\{100\}$ interface and $v^D = 0.46 \text{ m} \cdot \text{s}^{-1}$ for the $\{110\}$ interface. The values obtained
 333 here are an order of magnitude lower than the values obtained from the CGM and the local non-equilibrium
 334 model of Galenko and Sobolev [53] reported by Yang et al., which fall between $1.3 - 1.6 \text{ m} \cdot \text{s}^{-1}$ [8].

335 Using the values of v^D and the definition $v^D = D^I/\delta$, the magnitude of the trans-interface diffusion
 336 coefficient can be estimated. While the exact values of δ for Ni-Cu interfaces are not reported in Ref. [8],
 337 Monte-Carlo simulations by Ramalingam et al. [54] report equilibrium “10-90” interface widths of $7.2 \pm 0.9 \text{ \AA}$
 338 for $\{100\}$ and $\{111\}$ orientations in Ni-Cu. Here, we assume that the interface width is independent of

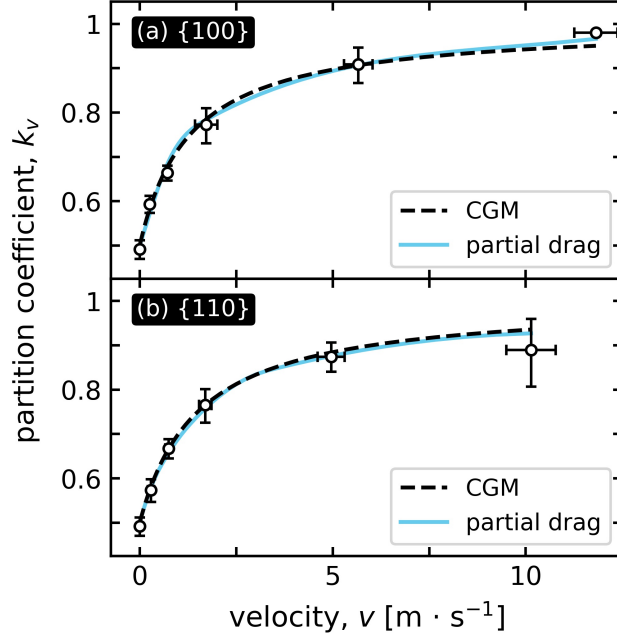


Figure 4: Fitting the distribution coefficient to the concentration response function, Eq. (31), for (a) $\{100\}$ and (b) $\{110\}$ interfaces, with comparison to the CGM. Open circles are the results from the molecular dynamics simulations of Ni-Cu by Yang et al. [8].

velocity, which is reasonable for the velocity range analyzed here, but perhaps not so for v approaching the diffusive speed in the bulk liquid [26]. Using the values of v^D obtained from the CGM and the local non-equilibrium model gives $D^I = 0.94 - 1.15 \times 10^{-9} \text{ m}^2 \cdot \text{s}^{-1}$, which are equivalent to typical diffusive speeds in a metallic melt, $D^I \sim 10^{-9} \text{ m}^2 \cdot \text{s}^{-1}$. In contrast, the values of v^D from the present model give values of $D^I = 2.3 \times 10^{-10} \text{ m}^2 \cdot \text{s}^{-1}$ for the $\{100\}$ interface and $D^I = 3.3 \times 10^{-10} \text{ m}^2 \cdot \text{s}^{-1}$ for the $\{110\}$ interface. These values are between the typical diffusivities in bulk solids and metallic melts, which agrees with the behavior intuitively expected for a solid/liquid interface. A more in-depth study on the nature of diffusion through the interface will be reported elsewhere [55]. The reason for this improved prediction is evident from Figure 2 — to predict a given amount of solute trapping, v^D must decrease if λ decreases.

3.2. Calculation of non-equilibrium phase boundaries

The interfacial response functions can also provide the temperature of the interface. However, the standard expression for the interfacial temperature [56, 57, 58, 59] and its partial-drag extension [19] is obtained by linearizing Eq. (30) in the concentration, i.e., by assuming a dilute-ideal solution. Here, to illustrate the effects of partial solute drag in a non-ideal, non-dilute alloy, the non-equilibrium solidus and liquidus curves for the Ag-Cu system are calculated by solving the full interfacial response functions for x_b^s and x_b^l at various values of T and λ .

To apply the present model to this binary alloy, we again use Eqs. (30) and (31). We also examine the widely used CGM of Aziz and Kaplan [18], which uses reaction rate theory to derive the interfacial response

functions for a binary alloy, which can be written as:

$$x_b^{eff} \llbracket \mu_b \rrbracket + (1 - x_b^{eff}) \llbracket \mu_a \rrbracket = -RT \ln \left\{ 1 - \frac{v}{v_0} \right\} \quad (37)$$

$$\llbracket \mu_a \rrbracket - \llbracket \mu_b \rrbracket = -RT \ln \left\{ 1 - \frac{x_b^l - x_b^s}{x_b^s(1 - x_b^l)} \cdot \frac{v}{v^D} \right\} \quad (38)$$

Using the free energies for Ag-Cu from Murray [60] in Thermo-Calc software [61, 62] to evaluate the chemical potentials, the systems of Eqs. (30)–(31) for the present model and (37)–(38) for the Aziz and Kaplan model [18] are solved at various values of temperature, T , and solute-drag parameter, λ , to obtain x_{Cu}^s and x_{Cu}^l . We fix $v = 0.1 \text{ m} \cdot \text{s}^{-1}$ and, as a first approximation, use kinetic parameters on the order of the results found in Section 3.1: $v^D = 0.4 \text{ m} \cdot \text{s}^{-1}$ and $v_0 = 850 \text{ m} \cdot \text{s}^{-1}$. A simplex method [63] is implemented to solve these non-linear systems, yielding the kinetic phase diagrams in Figure 5, where 5(a) and 5(b) correspond to the present model and 5(c) and 5(d) correspond to the Aziz and Kaplan model.

The present model is symmetric with respect to the a and b species, meaning that one can either decide to consider a to be Cu and b to be Ag or vice-versa without modifying the equations and their solutions. This behavior is inherent to the mathematical formulation of Eqs. (30)–(31), and is also consistent with the expectation that the $\text{Ag}_{(x_a=x)}\text{Cu}_{(x_b=1-x)}$ alloy gives the same solution as the $\text{Cu}_{(x_a=1-x)}\text{Ag}_{(x_b=x)}$ alloy. Consequently, the results displayed in Fig. 5a and 5b combine calculations using both Cu and Ag as component b , and are able to fully capture the retrograde solidus behavior observed in this system at local equilibrium.

The Aziz and Kaplan model is asymmetric with respect to the choice of component a and b due to the use of reaction-rate theory in the development of their CRF, which describes the exchange of a b atom in the solid with an a atom in the liquid under exponential kinetics. Upon replacing all values of x_b in Eqs. (37)–(38) with x_a and vice-versa, Eq. (37) remains the same, while the right-hand side of (38) becomes $RT \ln\{1 + \dots\}$. While the relationship $\ln(1 - \epsilon) \approx -\epsilon$ can be used to linearize Eq. (38) in the limit of $v \ll v^D$, the asymmetry remains due to the use of $x_b^s x_a^l$ to describe the trans-interface mobility. Thus, the choice of species corresponding to components a and b will affect the resulting diagram, so one must decide on a methodology to draw the phase boundaries. Here, we have reproduced the kinetic phase diagrams published in Ref. [18] and reapplied the original methodology. For the Ag-rich domain shown in Fig. 5c, we solve Eqs. (37)–(38) with $a \simeq \text{Ag}$ and $b \simeq \text{Cu}$, only keeping solutions with $x_{Cu}^s \leq 0.5$. The Cu-rich domain shown in Figure 5d is solved with an analogous procedure, where $a \simeq \text{Cu}$ and $b \simeq \text{Ag}$ and only the solutions with $x_{Ag}^s \leq 0.5$ are retained. The results are further filtered to discard solutions where x^s falls inside the region of spinodal decomposition of the solid phase. The boundary of this region, shown by the dotted lines drawn in Figures 5c and 5d, is defined by the inflection points of the Gibbs free energy of the solid phase. This information is provided in Thermo-Calc software using the QF (*phase stability*) function [64].

The results of the present model and the Aziz and Kaplan model agree qualitatively in that increasing the amount of solute drag will depress the interfacial temperature for a given concentration and that the effect of this “solute-drag undercooling” becomes more significant as the concentration increases. However, the shapes of the calculated phase boundaries are remarkably different between the two models. Most notably, the Aziz and Kaplan model lacks any sort of retrograde solidus behavior, causing the solid compositions to

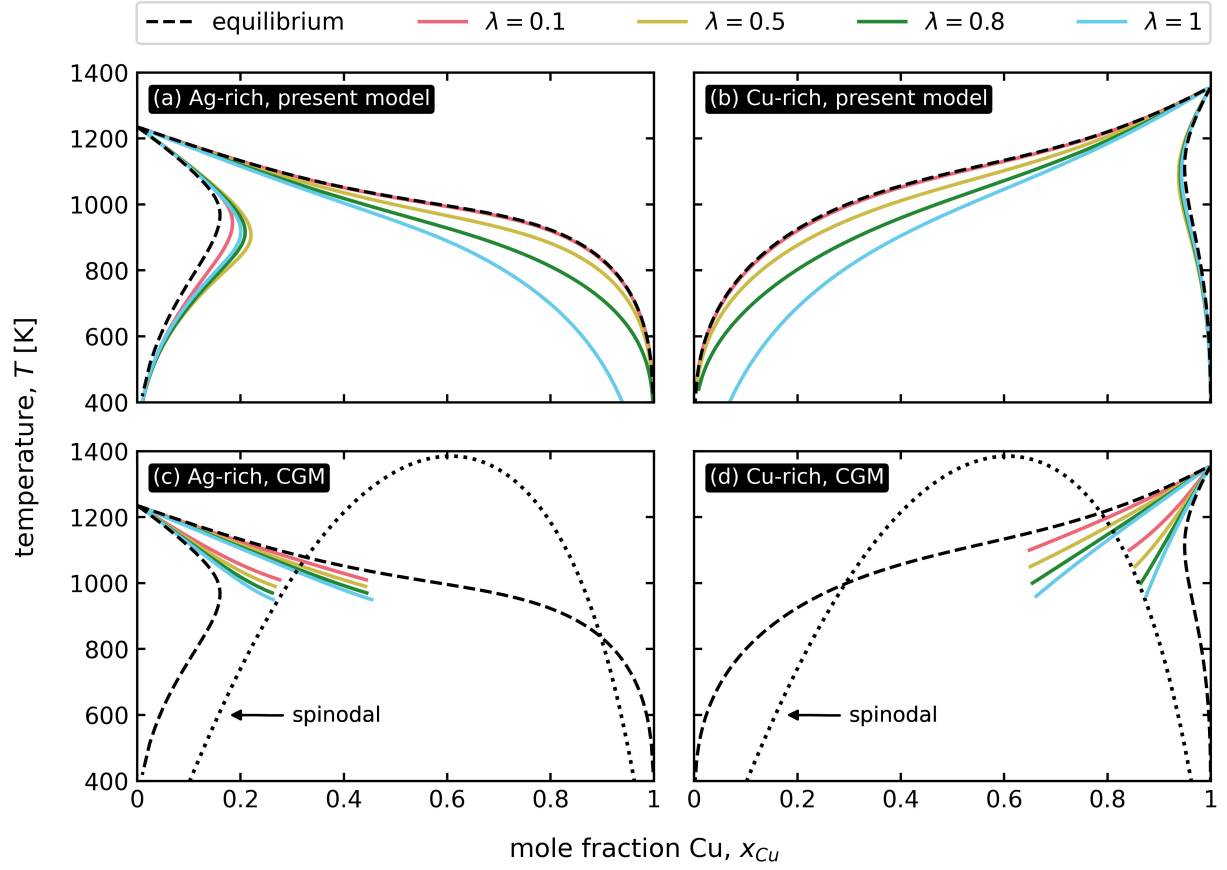


Figure 5: Kinetic phase boundaries for the Ag-Cu system as a function of the solute-drag parameter for $v = 0.1 \text{ m} \cdot \text{s}^{-1}$, $v^D = 0.4 \text{ m} \cdot \text{s}^{-1}$, and $v_0 = 850 \text{ m} \cdot \text{s}^{-1}$. The results of the present model, i.e., Eqs. (30) and (31), are shown in (a) and (b), and those of the CGM [18], i.e., Eqs. (37) and (38), are shown in (c) and (d). Only the boundaries where the compositions are stable, i.e., outside the spinodal of the solid phase (dotted lines), are shown. The equilibrium liquidus and solidus lines and their metastable extensions are shown with dashed lines.

quickly enter the spinodal, while the present model is able to capture the retrograde solidus behavior, so the phase boundaries never enter the region of spinodal decomposition at any values of λ examined here.

As $\lambda \rightarrow 0$, the factor of λ in the solute-drag flux of the present model (i.e., the left-hand side of Eq. (31)) becomes significant. While Aziz and Kaplan allow partial-solute drag to modify the driving force of each response function, they do not account for its effect on the solute-drag flux (i.e., the numerator of the log term in Eq. (38)), using $x_b^l - x_b^s$ for both the full- and zero-drag cases discussed in their analysis. This causes the kinetic phase boundaries to deviate significantly from the equilibrium phase boundaries, even for small amounts of solute drag. However, the presence of λ in the present model scales the solute-drag flux with the available driving force, and the concentrations approach their equilibrium values as $\lambda \rightarrow 0$ (although, as before, we must have $\lambda > 0$ to obey the dissipation inequality).

While the solute-drag fluxes of Eqs. (31) and (38) are equal when $\lambda = 1$, the choice of trans-interface mobility remains a differentiating factor between the two models. The Aziz model uses reaction-rate theory, leading to a concentration dependence given by $x_b^s x_a^l$, while the present model accounts for the effective concentration of the interface, as discussed in Section 2.3, leading to $x_b^l x_a^l$ when $\lambda = 1$. Notably, because the product $x_b^s x_a^l$ is asymmetric with respect to the choice of components a and b , the CGM is unable to capture the retrograde solidus behavior.

4. Discussion: Interpretations of solute drag in the context of binary alloys

To compare the current model with the other sharp-interface models available in the literature, it is instructive to take the constitutive laws derived using energy dissipation and re-interpret them with the classical approach using Gibbs free energy changes. To make the comparison as simple as possible, we use the expressions for a binary alloy and neglect cross-coupling, as given by Eqs. (18) and (19) in the binary limit. Using the dissipation inequality, it is possible to directly identify the driving forces ($\text{J} \cdot \text{mol}^{-1}$) for interface motion, $D^m = (M^m)^{-1}v$, and trans-interface diffusion, $D^t = (\rho_0 M_{bb}^t)^{-1}J_b^t$, in the binary limit. Although the driving forces in this limit are identical to those in Eqs. (30) and (31), there can be diffusion in both phases, i.e., a non-zero J_b^α term in Eq. (31). These driving forces can then be related to the Gibbs free energy changes for those processes as given by Hillert [35]:

$$\Delta G^p = D^p \Delta \xi^p \quad (39)$$

where $\Delta \xi^p$ is the “extent of the process” in moles per mole of material transformed and the superscript $p = \{m, t, tot\}$ denotes the relevant process. Thus, the free energy changes can vary with the model for the conditions at the interface.

These free energy changes are illustrated for the full-drag (subscript “*full*”), partial-drag (subscript “*eff*”), and partial drag from bulk diffusion (subscript “*tr*”) models in Figure 6a, 6b, and 6c, respectively. Various graphical constructions are used to calculate the Gibbs free energy changes for interface migration, ΔG^m (marked in red), and trans-interface diffusion, ΔG^t (marked in blue), for each model. The sum of these values of the total Gibbs free energy change for the $\beta \rightarrow \alpha$ transformation, $\Delta G^{tot} = \Delta G^m + \Delta G^t$ (marked in purple). We only show these constructions for the growing phase in order to emphasize the $\beta \rightarrow \alpha$ transformation.

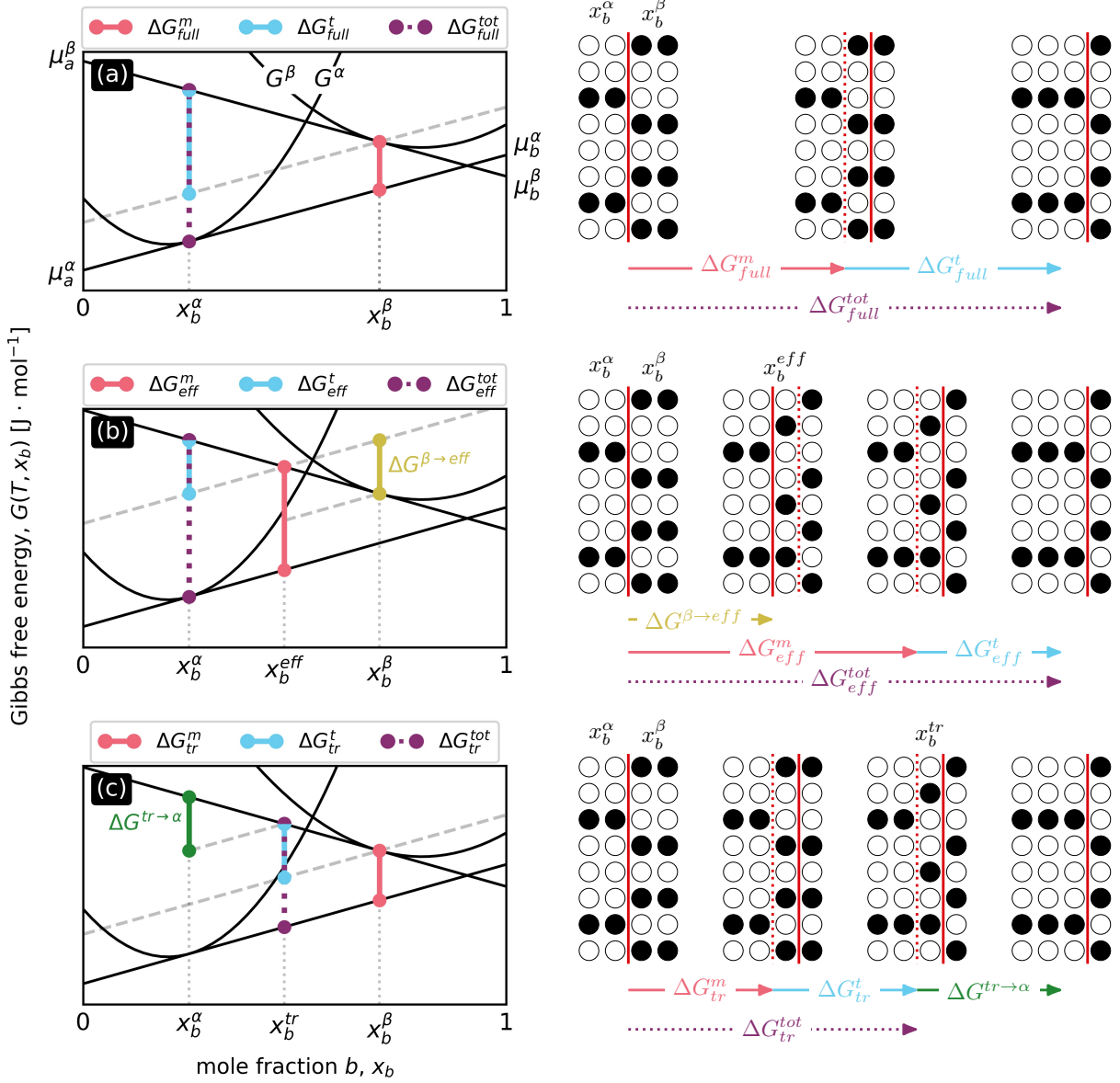


Figure 6: Graphical constructions and schematics for binary alloys showing the dissipative processes in the three classes of sharp-interface models incorporating solute drag: (a) the full-drag model in which material is adsorbed to the interface at x_b^β and transferred to the growing phase at x_b^α , (b) a partial-drag model in which the interface can adsorb material at $x_b^{eff} \neq x_b^\beta$, and (c) a partial-drag model in which material can be transferred to the growing phase at $x_b^{tr} \neq x_b^\beta$. Similarly, the first and last columns of the schematics are the same, corresponding to the initial and final distribution of (white dots) a and (black dots) b species in the (left) α growing and (right) β parent phases. Here, we set $x_b^{eff} = x_b^{tr}$ to facilitate comparison between the three approaches. In the graphical constructions, red vertical lines indicate ΔG^m , blue vertical lines indicate ΔG^t , and purple vertical lines indicate ΔG^{tot} for each class of model. In the schematics, solid red vertical lines denote the location of the sharp interface, and the dotted red line is used in conjunction with the solid red line to denote a transition state for which the process of concentration adjustment has yet to occur.

4.1. “Full-drag” models

With $\lambda = 1$ in the present model, we recover a class of sharp-interface models known as “full-drag models”. From Eq. (1), this sets $x_b^{eff} = x_b^\beta$, indicating that the motion of the interface dissipates ΔG_{full}^m by adsorbing $\Delta \xi_{full}^m = 1$ mole of material at composition x_b^β and that solute drag dissipates ΔG_{full}^t by desorbing $\Delta \xi_{full}^t = x_b^\beta - x_b^\alpha$ moles of b from the interface back to the parent phase. The overall $\beta \rightarrow \alpha$ phase transformation dissipates ΔG_{full}^{tot} and represents the growth of α at composition x_b^α from β at composition x_b^β . From the graphical construction in Figure 6a, these Gibbs free energy changes are

$$\Delta G_{full}^m = x_b^\beta [\mu_b] + (1 - x_b^\beta) [\mu_a] \quad (40)$$

$$\Delta G_{full}^t = (x_b^\beta - x_b^\alpha) ([\mu_a] - [\mu_b]) \quad (41)$$

$$\Delta G_{full}^{tot} = x_b^\alpha [\mu_b] + (1 - x_b^\alpha) [\mu_a] \quad (42)$$

and from Eq. (39), the corresponding driving forces for the two interfacial processes are

$$D_{full}^m = x_b^\beta [\mu_b] + (1 - x_b^\beta) [\mu_a] \quad (43)$$

$$D_{full}^t = [\mu_a] - [\mu_b] \quad (44)$$

Full-drag models were initially developed for binary alloys by Aziz and Kaplan [18] (the “with-drag” case of the CGM) and subsequently discussed by Hillert [35] and used by Rettenmayr and coworkers [65, 66]. Additionally, the full-drag flux is used by Galenko and Sobolev [49, 50, 53, 67, 68] in the framework of extended irreversible thermodynamics to discuss solute trapping in binary alloys with non-equilibrium diffusion in the liquid (β in the current notation). Galenko also performs analyses with extended irreversible thermodynamics using the full-drag driving forces [69, 70].

4.2. Partial-drag models motivated by rapid solidification (using x_b^{eff})

The present model allows λ in Eq. (1) to take any value permitted by the dissipation inequalities in Eqs. (13) and (14). In this case, the motion of the interface dissipates ΔG_{eff}^m by adsorbing $\Delta \xi_{eff}^m = 1$ mole of material at composition x_b^{eff} and that solute drag dissipates ΔG_{eff}^t by desorbing $\Delta \xi_{eff}^t = x_b^{eff} - x_b^\alpha$ moles of b from the interface back to the parent phase. The overall $\beta \rightarrow \alpha$ transformation dissipates ΔG_{eff}^{tot} and represents the growth of α at composition x_b^α from β at composition x_b^β . From the graphical construction in Figure 6b, these Gibbs free energy changes are

$$\Delta G_{eff}^m = x_b^{eff} [\mu_b] + (1 - x_b^{eff}) [\mu_a] \quad (45)$$

$$\Delta G_{eff}^t = (x_b^{eff} - x_b^\alpha) ([\mu_a] - [\mu_b]) \quad (46)$$

$$\Delta G_{eff}^{tot} = x_b^\alpha [\mu_b] + (1 - x_b^\alpha) [\mu_a] \quad (47)$$

and from Eq. (39), the corresponding driving forces for the two interfacial processes are identical to those of the present model in the case of a binary alloy with a planar interface, i.e., those in Eqs. (30) and (31):

$$D_{eff}^m = x_b^{eff} [\mu_b] + (1 - x_b^{eff}) [\mu_a] \quad (48)$$

$$D_{eff}^t = [\mu_a] - [\mu_b] \quad (49)$$

These driving forces can also be obtained directly from the energy dissipation approach, as shown in Appendix A. Comparing Figures 6a and 6b, it is evident that ΔG_{eff}^m is greater than ΔG_{full}^m and that ΔG_{eff}^t is less than ΔG_{full}^t by the same amount. Eq. (45) can be rewritten as

$$\Delta G_{eff}^m = x_b^\beta [\mu_b] + (1 - x_b^\beta) [\mu_a] + (x_b^\beta - x_b^{eff}) ([\mu_a] - [\mu_b]) \quad (50)$$

This difference in energy, $\Delta G^{\beta \rightarrow eff}$, is marked in yellow on Figure 6b and given by

$$\Delta G^{\beta \rightarrow eff} = (x_b^\beta - x_b^{eff}) ([\mu_a] - [\mu_b]) \quad (51)$$

and is the energy required to adjust the concentration ahead of the interface so the interface can adsorb material at x_b^{eff} instead of x_b^β . From Eq. (50), we can see that adsorbing one mole of material to the interface at x_b^{eff} dissipates an amount of energy equivalent to that dissipated by both adsorbing one mole of material at x_b^β and displacing $\Delta \xi^{\beta \rightarrow eff} = x_b^\beta - x_b^{eff}$ moles in the liquid ahead of the advancing interface. This clearly makes the process of interface motion more difficult, but because $\Delta \xi^{\beta \rightarrow eff}$ must no longer be desorbed from the interface, less energy is required by the solute-drag process. Physically, the expressions for ΔG_{eff}^t and ΔG_{eff}^m are obtained by simply transferring the energy $\Delta G^{\beta \rightarrow eff}$ from ΔG_{full}^t to ΔG_{full}^m . This has no effect on the total energy dissipated by the net transformation, as Eq. (47) is identical to Eq. (42), and remains conceptually consistent with Eq. (5), where the net mass transfer is independent of x_b^{eff} .

The first use of the variable solute-drag parameter as defined in Eq. (1) is due to the rapid solidification model of Aziz and Boettinger [19], who extended the full-drag case of the CGM to partial drag by multiplying ΔG^t by the solute-drag parameter, λ , which was assumed to lie between $0 \leq \lambda \leq 1$ (i.e., $x_b^\alpha \leq x_b^{eff} \leq x_b^\beta$). However, they did not incorporate λ in the flux of their CRF; hence, the expression for k_v in the widely used CGM is independent of the solute-drag parameter, as discussed in Sections 3.1 and 3.2. Another sharp-interface model incorporating a solute-drag parameter was developed by Li et al. [25] by extending Galenko's full-drag model [69] to the case of partial solute drag and concentrated solutions, although their analysis is limited to binary alloys without diffusion in the growing phase, while the present model can treat multicomponent alloys with diffusion in both phases.

4.3. Partial-drag models motivated by solid-state transformations (using x^{tr})

As in the present model, other sharp-interface models allow for bulk diffusion on both sides of the interface, which is essential for modeling solid-state phase transformations. The approach of Hillert, Rettenmayr, and coworkers [13, 14, 71, 72, 73] differs from those previously described in that a composition x_b^{tr} (x^i or x^{trans} in their notation) is used to represent “the composition of material actually transferred across the interface” [13]. We refer to models using this interpretation as *partial-drag models from bulk diffusion*, as this composition is not defined with a solute-drag parameter, as in Eq. (1), but by the bulk fluxes of component b near the interface in each phase, J_b^ϕ , as [13, 14]:

$$x_b^{tr} = \frac{x_b^\alpha J_b^\beta - x_b^\beta J_b^\alpha}{J_b^\beta - J_b^\alpha} \quad (52)$$

One limitation of this approach arises immediately from the definition of x_b^{tr} ; if diffusion does not occur in the growing phase (i.e., $J_b^\alpha = 0$), Eq. (52) gives $x_b^{tr} = x_b^\alpha$. Thus, when solid-state diffusion can be

reasonably neglected, as in rapid solidification, this model reduces to the full-drag case described in Section 4.1. While this may have initially seemed a reasonable assumption, the inability to treat partial solute drag during solidification implies that the model cannot be used to describe relatively recent molecular dynamics simulations of rapid solidification [8, 9], and thus does not recover the predictions of the partial-drag models described above.

In general, the interpretation of the interfacial processes differs from that of the present model. In partial-drag models from bulk diffusion, the motion of the interface dissipates ΔG_{tr}^m by adsorbing $\Delta \xi_{tr}^m = 1$ mole of material at composition x_b^β and that solute drag dissipates ΔG_{tr}^t by desorbing $\Delta \xi_{tr}^t = x_b^\beta - x_b^{tr}$ moles of b from the interface back to the parent phase. The overall $\beta \rightarrow \alpha$ transformation dissipates ΔG_{tr}^{tot} , but unlike the previous models, does not necessarily represent the growth of α at composition x_b^β from β at composition x_b^β . From the graphical construction in Figure 6c, these Gibbs free energy changes are

$$\Delta G_{tr}^m = x_b^\beta [\mu_b] + (1 - x_b^\beta) [\mu_a] \quad (53)$$

$$\Delta G_{tr}^t = (x_b^\beta - x_b^{tr}) ([\mu_a] - [\mu_b]) \quad (54)$$

$$\Delta G_{tr}^{tot} = x_b^{tr} [\mu_b] + (1 - x_b^{tr}) [\mu_a] \quad (55)$$

and from Eq. (39), the corresponding driving forces for the two interfacial processes are

$$D_{tr}^m = x_b^\beta [\mu_b] + (1 - x_b^\beta) [\mu_a] \quad (56)$$

$$D_{tr}^t = [\mu_a] - [\mu_b] \quad (57)$$

Comparing Eqs. (42), (47), and (55), it is evident that ΔG_{tr}^{tot} is less than both ΔG_{full}^{tot} and ΔG_{eff}^{tot} by the same amount:

$$\Delta G^{tr \rightarrow \alpha} = (x_b^{tr} - x_b^\alpha) ([\mu_a] - [\mu_b]) \quad (58)$$

which is also marked in green on Figure 6c. Although x_b^{tr} is described as the composition of the material transferred across the interface, it is not the interfacial composition of the solid (unless $x_b^{tr} = x_b^\alpha$), as the solid tangent in Figure 6c is drawn from x_b^α regardless of the value of x_b^{tr} . Evidently, the material at x_b^{tr} is still in the interface, yet the redistribution of $\Delta \xi^{tr \rightarrow \alpha}$ is not considered to dissipate energy at the interface, as it is clear from both Eq. (55) and Figure 6c that the total driving force only considers the transformation to the composition x_b^{tr} . In the present model, the flux between the interfacial control volume and the bulk growing phase is incorporated in the dissipation by solute drag via the J^α term in the CRF.

These differences between the partial-drag models and partial-drag models from bulk diffusion are due to different interpretations of solute drag. Note that $\Delta G^{tr \rightarrow \alpha}$ is exactly ΔG_{eff}^t (with x_b^{eff} replacing x_b^β), and that $\Delta G^{\beta \rightarrow eff}$ is exactly ΔG_{tr}^t . The partial-drag models assume that material can be adsorbed at $x_b^{eff} < x_b^\beta$, and that solute drag adjusts the adsorbed concentration to the interfacial concentration of the growing phase. The partial-drag models further assume that the redistribution $\Delta \xi^{\beta \rightarrow eff}$ ahead of the advancing interface is not solute drag, but necessary for the motion of the interface. Contrarily, the partial-drag models from bulk diffusion assume that material must be adsorbed at x_b^β , and that solute drag adjusts this adsorbed material to the composition that is incorporated into the growing phase at some composition x_b^{tr} , which is not necessarily equal to x_b^α . However, the energy dissipated by the adjusting x_b^{tr} to x_b^α , $\Delta G^{tr \rightarrow \alpha}$,

is not considered to be solute drag or contribute to the total energy dissipated at the interface, except in the two-step solute-drag process described by Kuang et al. [30]; even then, ΔG^m is modified such that the total driving force for the phase transformation is still given by Eq. (55).

The partial-drag models from bulk diffusion have been extended to describe highly non-equilibrium solidification by Wang and coworkers [27, 31, 74, 46, 51], which apply the maximal entropy production principle and consider non-equilibrium bulk diffusion in both the solid and the liquid. In the present model, we simply require that the response functions ensure that the energy decreases with interfacial motion, i.e., they are consistent with the dissipation inequalities, Eqs. (13) and (14). In contrast, the maximal entropy production approach assumes that the process dissipates the free energy at the fastest possible rate. The present model is unable to recover the results of these analyses, as they report that partial solute drag is inconsistent with the maximal entropy production principle [27]. However, a partial-solute drag model is briefly proposed in Ref. [27] as a “simplified treatment for the diffuse interface” with the following driving forces:

$$D^m = x_b^{eff} \llbracket \mu_b \rrbracket + (1 - x_b^{eff}) \llbracket \mu_a \rrbracket \quad (59)$$

$$D^t = \gamma (\llbracket \mu_a \rrbracket - \llbracket \mu_b \rrbracket) \quad (60)$$

where γ is analogous to λ , ranging from $0 < \gamma \leq 1$ to weight x_b^{eff} from x_b^{tr} to x_b^β . The driving force D^m is the same as the present model, i.e., Eq. (48), but the driving force D^t differs from that of the present model, i.e., Eq. (49).

4.4. Comparison to diffuse-interface approaches

We now show how the various sharp-interface models can be recovered from the classical diffuse-interface models. From Hillert’s reformulation [71] of the classical Cahn result [75], the dissipation due to interfacial motion can be written as

$$\Delta G_{diff}^m = \int_0^\delta \sum_{i=1}^N x_i \frac{d(\mu_i - \mu_i^\alpha)}{d\eta} d\eta \quad (61)$$

where both x_i and μ_i are functions of position within the diffuse interface, η , where $\eta < 0$ is the bulk α phase and $\eta > \delta$ is the bulk β phase. From Hillert [71], the classical Hillert and Sundman result [20], representing the dissipation due to solute drag, can be generalized to

$$\Delta G_{diff}^t = - \int_0^\delta \sum_{i=1}^N (x_i - x_i^\alpha) \frac{d\mu_i}{d\eta} d\eta \quad (62)$$

As in the sharp-interface models from the previous sections, Eqs. (61) and (62) must sum to the total free energy change for the $\beta \rightarrow \alpha$ transformation:

$$\Delta G_{diff}^{tot} = \int_0^\delta \sum_{i=1}^N x_i \frac{d(\mu_i - \mu_i^\alpha)}{d\eta} d\eta - \int_0^\delta \sum_{i=1}^N (x_i - x_i^\alpha) \frac{d\mu_i}{d\eta} d\eta \quad (63)$$

538 Using the Gibbs-Duhem relation, $\sum_{i=1}^N x_i d\mu_i^\alpha = 0$, gives

$$\Delta G_{diff}^{tot} = \int_0^\delta \sum_{i=1}^N x_i \frac{d\mu_i}{d\eta} d\eta - \int_0^\delta \sum_{i=1}^N (x_i - x_i^\alpha) \frac{d\mu_i}{d\eta} d\eta \quad (64)$$

$$= \int_0^\delta \sum_{i=1}^N x_i^\alpha \frac{d\mu_i}{d\eta} d\eta \quad (65)$$

539 Because x_i^α is constant in the sharp interface limit, i.e., $\delta \rightarrow 0$, Eq. (65) becomes

$$\Delta G_{diff}^{tot} = \sum_{i=1}^N x_i^\alpha [\mu_i] \quad (66)$$

540 which is identical to the total Gibbs free energy change of the present model, i.e., the multicomponent
 541 extension of Eq. (47), and also that of the full-drag model, Eq. (42). The partial-drag models from bulk
 542 diffusion opt to use x_i^{tr} instead of x_i^α in Eq. (62), leading to a different total driving force when diffusion
 543 can occur in the growing phase.

544 The original formulation of Cahn's result [75] has also been extended for grain growth by Alkayyali and
 545 Abdeljawad [76], who add an additional term that results from considering asymmetric solute segregation at
 546 grain boundaries by incorporating a regular solution model. Furthermore, Li et al. [26] extend the Hillert-
 547 Sundman result [20] to include local non-equilibrium liquid diffusion by following Galenko's treatment [67]. Li
 548 et al. also incorporate partial solute drag and find it necessary to reproduce the experimental measurements
 549 of Si-9As by Kittl et al. [77]. While diffuse-interface models are inherently more detailed, sharp-interface
 550 models avoid the uncertainty of interpolating properties through the interface. The present model provides
 551 a convenient way to add detail to a sharp-interface model through the solute-drag parameter with only a
 552 small increase in complexity. Work on solid-state transformations in steels [78, 79] has shown that interface
 553 kinetics depend heavily on the choice of potential well for solutes at the interface, inviting a comparison to
 554 the solute-drag parameter, λ , in the present sharp-interface model. This parameter could be derived from a
 555 diffuse-interface model simply by evaluating Eq. (61) or Eq. (62) and comparing to Eq. (45) or Eq. (46),
 556 respectively. Because the total free energy change for the transformation is independent of the degree of
 557 solute drag, the parameters λ , $x_i(\eta)$, and $\mu_i(\eta)$ must be specified such that $\Delta G_{diff}^m + \Delta G_{diff}^t = \Delta G_{diff}^{tot} =$
 558 ΔG_{eff}^{tot} in order to draw a comparison between a diffuse-interface model and the present sharp-interface
 559 model.

560 5. Conclusion

561 A dissipation relation for the free energy is used to drive thermodynamically consistent interfacial re-
 562 sponse functions for the interfacial compositions and velocity during phase transformations in concentrated
 563 multicomponent alloys. The theory accounts for solute drag at the interface and diffusion in both phases, and
 564 is applicable to both solid/solid and solid/liquid transformations. The potential for cross-coupling between
 565 the dissipative processes at the interface is presented. Even when cross-coupling is neglected, the driving
 566 force for the motion of the interface is a function of both the grand potential and the diffusion potentials

for each independent component. Both the interfacial velocity and compositions (e.g., the distribution coefficient) depend on the degree of solute drag. In the current formulation, the cumulative effect of solute drag on a multicomponent system is described by a single value of the solute drag parameter, which can be determined by fitting the interfacial response functions to experimental or simulation data. However, the solute drag parameter could also be a function of composition, and the limits to this parameter that are consistent with energy dissipation are given. Additionally, effects such as interfacial energy, interfacial energy anisotropy, elastic stress, and non-equilibrium bulk diffusion can be incorporated via additional terms in the dissipation relation, which naturally yields interface response functions for these various cases.

The interfacial response functions are simplified to the case of the rapid solidification of a binary alloy with the goal of describing the conditions at solid/liquid interfaces during additive manufacturing. Due to the dependence of the distribution coefficient on the degree of solute drag, we find that the present partial-drag model yields more reasonable estimates of trans-interface diffusivities than do full-drag models. Additionally, the response functions are used to calculate non-equilibrium phase boundaries in Ag-Cu, in which increasing the amount of solute drag increases the amount of kinetic undercooling for a given concentration. The phase boundaries calculated with the present model significantly deviate from the predictions of other widely used models, and the present model is able to capture the retrograde solidus curves at all values of the solute-drag parameter examined here. These findings indicate that the effects of partial solute drag are important at solidification velocities relevant to additive manufacturing.

Declaration of competing interest

The authors declare that they have no known competing financial interests or personal relationships that could have appeared to influence the work reported in this paper.

Acknowledgements

CAH acknowledges support from the National Science Foundation Graduate Research Fellowship (grant number DGE-1842165) and from the Ryan Fellowship at the International Institute for Nanotechnology. PWV acknowledges the financial assistance award 70NANB14H012 from the U.S. Department of Commerce, National Institute of Standards and Technology as part of the Center for Hierarchical Materials Design (CHiMaD), as well as support from the Fédération Doebelin for a visit at CEMEF, a research center of Mines Paris.

Appendices

A. The interfacial response functions for a rapidly solidifying binary alloy

A.1. Velocity response function

Neglecting cross-coupling, the VRF for a multicomponent alloy is given by Eq. (18) in the main text:

$$v = M^m \rho_0^{-1} \left(\llbracket \Omega_v \rrbracket + \rho_0 \sum_{k=2}^N x_k^{eff} \llbracket \tilde{\mu}_k \rrbracket \right) \quad (18)$$

For a binary alloy ($a = 1, b = 2$), this becomes

$$v = M^m \left(\rho_0^{-1} \llbracket \Omega_v \rrbracket + x_b^{eff} \llbracket \mu_b - \mu_a \rrbracket \right) \quad (A.1)$$

Using Eq. (12) to expand the grand potential yields

$$v = M^m \left(\llbracket \rho_0^{-1} f_v - (\mu_b - \mu_a) x_b \rrbracket + x_b^{eff} \llbracket \mu_b - \mu_a \rrbracket \right) \quad (A.2)$$

Expanding the jumps yields

$$v = M^m \left(\rho_0^{-1} f_v^l - (\mu_b^l - \mu_a^l) x_b^l - \rho_0^{-1} f_v^s + (\mu_b^s - \mu_a^s) x_b^s + x_b^{eff} [\mu_b^l - \mu_a^l - \mu_b^s + \mu_a^s] \right) \quad (A.3)$$

For a system at constant temperature and volume, the bulk Helmholtz free energies are given by:

$$\rho_0^{-1} f_v^\phi = \mu_a^\phi x_a^\phi + \mu_b^\phi x_b^\phi \quad (A.4)$$

which gives

$$v = M^m \left(\mu_a^l - \mu_a^s + x_b^{eff} [\mu_b^l - \mu_a^l - \mu_b^s + \mu_a^s] \right) \quad (A.5)$$

$$= M^m \left(x_b^{eff} \llbracket \mu_b \rrbracket + (1 - x_b^{eff}) \llbracket \mu_a \rrbracket \right) \quad (A.6)$$

Using M^m from Eq. (20) yields the VRF for the rapid solidification of a binary alloy in Eq. (30).

A.2. Concentration response function

Neglecting cross-coupling, the CRF for a multicomponent alloy is given by Eq. (19) in the main text:

$$J_i^t = -\rho_0 \sum_{j=2}^N M_{ij}^t \llbracket \tilde{\mu}_j \rrbracket \quad (19)$$

For a binary alloy ($a = 1, b = 2$), the solute-drag flux of component b is given by

$$J_b^t = -\rho_0 M_{bb}^t \llbracket \mu_b - \mu_a \rrbracket \quad (A.7)$$

Expanding the jump yields

$$J_b^t = -\rho_0 M_{bb}^t (\mu_b^l - \mu_a^l - \mu_b^s + \mu_a^s) \quad (A.8)$$

$$= \rho_0 M_{bb}^t (\llbracket \mu_a \rrbracket - \llbracket \mu_b \rrbracket) \quad (A.9)$$

Using Eq. (3) with $J_b^\alpha = 0$ yields

$$v(x_b^{eff} - x_b^s) = M_{bb}^t (\llbracket \mu_a \rrbracket - \llbracket \mu_b \rrbracket) \quad (A.10)$$

Using M_{bb}^t from Eq. (25) yields the CRF for the rapid solidification of a binary alloy in Eq. (31).

References

- [1] D. Herzog, V. Seyda, E. Wycisk, C. Emmelmann, Additive manufacturing of metals, *Acta Materialia* 117 (2016) 371–392. doi:10.1016/j.actamat.2016.07.019.
- [2] W. J. Sames, F. A. List, S. Pannala, R. R. Dehoff, S. S. Babu, The metallurgy and processing science of metal additive manufacturing, *International Materials Reviews* 61 (5) (2016) 315–360. doi:10.1080/09506608.2015.1116649.
- [3] T. DebRoy, H. Wei, J. Zuback, T. Mukherjee, J. Elmer, J. Milewski, A. Beese, A. Wilson-Heid, A. De, W. Zhang, Additive manufacturing of metallic components – Process, structure and properties, *Progress in Materials Science* 92 (2018) 112–224. doi:10.1016/j.pmatsci.2017.10.001.
- [4] G. Boussinot, M. Apel, J. Zielinski, U. Hecht, J. Schleifenbaum, Strongly out-of-equilibrium columnar solidification during laser powder-bed fusion in additive manufacturing, *Physical Review Applied* 11 (1) (2019) 014025. doi:10.1103/PhysRevApplied.11.014025.
- [5] D. R. Gunasegaram, I. Steinbach, Modelling of microstructure in metal additive manufacturing: Recent progress, research gaps, and perspectives, *Metals* 11 (9) (2021) 1425. doi:10.3390/met11091425.
- [6] J. T. McKeown, K. Zweier, C. Liu, D. R. Coughlin, A. J. Clarke, J. K. Baldwin, J. W. Gibbs, J. D. Roehling, S. D. Imhoff, P. J. Gibbs, D. Tournet, J. M. K. Wiezorek, G. H. Campbell, Time-resolved in situ measurements during rapid alloy solidification: Experimental insight for additive manufacturing, *JOM* 68 (3) (2016) 985–999. doi:10.1007/s11837-015-1793-x.
- [7] V. Bathula, C. Liu, K. Zweier, J. McKeown, J. M. Wiezorek, Interface velocity dependent solute trapping and phase selection during rapid solidification of laser melted hypo-eutectic Al-11at.%Cu alloy, *Acta Materialia* 195 (2020) 341–357. doi:10.1016/j.actamat.2020.04.006.
- [8] Y. Yang, H. Humadi, D. Buta, B. B. Laird, D. Sun, J. J. Hoyt, M. Asta, Atomistic Simulations of Nonequilibrium Crystal-Growth Kinetics from Alloy Melts, *Physical Review Letters* 107 (2) (2011) 025505. doi:10.1103/PhysRevLett.107.025505.
- [9] S. Kavousi, B. R. Novak, J. Hoyt, D. Moldovan, Interface kinetics of rapid solidification of binary alloys by atomistic simulations: Application to Ti-Ni alloys, *Computational Materials Science* 184 (2020) 109854. doi:10.1016/j.commatsci.2020.109854.
- [10] T. Pinomaa, J. M. McKeown, J. M. Wiezorek, N. Provatas, A. Laukkanen, T. Suhonen, Phase field modeling of rapid resolidification of Al-Cu thin films, *Journal of Crystal Growth* 532 (2020) 125418. doi:10.1016/j.jcrysgro.2019.125418.
- [11] S. Kavousi, M. Asle Zaeem, Quantitative phase-field modeling of solute trapping in rapid solidification, *Acta Materialia* 205 (2021) 116562. doi:10.1016/j.actamat.2020.116562.
- [12] H. Humadi, J. J. Hoyt, N. Provatas, Phase-field-crystal study of solute trapping, *Physical Review E* 87 (2) (2013) 022404, publisher: American Physical Society. doi:10.1103/PhysRevE.87.022404.
- [13] M. Hillert, M. Rettenmayr, Deviation from local equilibrium at migrating phase interfaces, *Acta Materialia* 51 (10) (2003) 2803–2809. doi:10.1016/S1359-6454(03)00085-5.
- [14] M. Hillert, J. Odqvist, J. Ågren, Interface conditions during diffusion-controlled phase transformations, *Scripta Materialia* 50 (4) (2004) 547–550. doi:10.1016/j.scriptamat.2003.10.027.
- [15] M. Hillert, An application of irreversible thermodynamics to diffusional phase transformations, *Acta Materialia* 54 (1) (2006) 99–104. doi:10.1016/j.actamat.2005.08.023.
- [16] M. J. Aziz, Model for solute redistribution during rapid solidification, *Journal of Applied Physics* 53 (2) (1982) 1158–1168. doi:10.1063/1.329867.
- [17] M. J. Aziz, Dissipation-theory treatment of the transition from diffusion-controlled to diffusionless solidification, *Applied Physics Letters* 43 (6) (1983) 552–554. doi:10.1063/1.94416.
- [18] M. J. Aziz, T. Kaplan, Continuous growth model for interface motion during alloy solidification, *Acta Metallurgica* 36 (8) (1988) 2335–2347. doi:10.1016/0001-6160(88)90333-1.
- [19] M. Aziz, W. Boettinger, On the transition from short-range diffusion-limited to collision-limited growth in alloy solidification, *Acta Metallurgica et Materialia* 42 (2) (1994) 527–537. doi:10.1016/0956-7151(94)90507-X.
- [20] M. Hillert, B. Sundman, A treatment of the solute drag on moving grain boundaries and phase interfaces in binary alloys, *Acta Metallurgica* 24 (8) (1976) 731–743. doi:10.1016/0001-6160(76)90108-5.
- [21] N. A. Ahmad, A. A. Wheeler, W. J. Boettinger, G. B. McFadden, Solute trapping and solute drag in a phase-field model of rapid solidification, *Physical Review E* 58 (3) (1998) 3436–3450. doi:10.1103/PhysRevE.58.3436.

- [22] S. G. Kim, Y. B. Park, Grain boundary segregation, solute drag and abnormal grain growth, *Acta Materialia* 56 (15) (2008) 3739–3753. doi:10.1016/j.actamat.2008.04.007.
- [23] K. Eckler, D. M. Herlach, M. J. Aziz, Search for a solute-drag effect in dendritic solidification, *Acta Metallurgica et Materialia* 42 (3) (1994) 975–979. doi:10.1016/0956-7151(94)90291-7.
- [24] C. R. Hutchinson, H. S. Zurob, Y. Bréchet, The growth of ferrite in Fe-C-X alloys: The role of thermodynamics, diffusion, and interfacial conditions, *Metallurgical and Materials Transactions A* 37 (6) (2006) 1711–1720. doi:10.1007/s11661-006-0114-y.
- [25] S. Li, J. Zhang, P. Wu, A comparative study on migration of a planar interface during solidification of non-dilute alloys, *Journal of Crystal Growth* 312 (7) (2010) 982–988. doi:10.1016/j.jcrysgro.2009.12.070.
- [26] S. Li, J. Zhang, P. Wu, Numerical solution and comparison to experiment of solute drag models for binary alloy solidification with a planar phase interface, *Scripta Materialia* 62 (9) (2010) 716–719. doi:10.1016/j.scriptamat.2010.01.041.
- [27] H. Wang, F. Liu, H. Zhai, K. Wang, Application of the maximal entropy production principle to rapid solidification: A sharp interface model, *Acta Materialia* 60 (4) (2012) 1444–1454. doi:10.1016/j.actamat.2011.11.038.
- [28] A. Ludwig, The interface response-functions in multi-component alloy solidification, *Physica D: Nonlinear Phenomena* 124 (1-3) (1998) 271–284. doi:10.1016/S0167-2789(98)00202-4.
- [29] S. L. Sobolev, L. V. Poluyanov, F. Liu, An analytical model for solute diffusion in multicomponent alloy solidification, *Journal of Crystal Growth* 395 (2014) 46–54. doi:10.1016/j.jcrysgro.2014.03.009.
- [30] W. Kuang, H. Wang, J. Zhang, F. Liu, Application of the thermodynamic extremal principle to diffusion-controlled phase-transformations in multi-component substitutional alloys: Modeling and applications, *Acta Materialia* 120 (2016) 415–425. doi:10.1016/j.actamat.2016.08.078.
- [31] K. Wang, H. Wang, F. Liu, H. Zhai, Modeling rapid solidification of multi-component concentrated alloys, *Acta Materialia* 61 (4) (2013) 1359–1372. doi:10.1016/j.actamat.2012.11.013.
- [32] Q. Du, A. S. Azar, M. M’Hamdi, Kinetic interface condition phase diagram for the rapid solidification of multi-component alloys with an application to additive manufacturing, *Calphad* 76 (2022) 102365. doi:10.1016/j.calphad.2021.102365.
- [33] Q. Du, M. M’Hamdi, Predicting kinetic interface condition for austenite to ferrite transformation by multi-component continuous growth model, *Calphad* 77 (2022) 102423. doi:10.1016/j.calphad.2022.102423.
- [34] M. E. Gurtin, P. W. Voorhees, The thermodynamics of evolving interfaces far from equilibrium, *Acta Materialia* 44 (1) (1996) 235–247. doi:https://doi.org/10.1016/S1359-6454(95)00139-X.
- [35] M. Hillert, Solute drag, solute trapping, and diffusional dissipation of Gibbs energy, *Acta Materialia* 47 (18) (1999) 4481–4505. doi:https://doi.org/10.1016/S1359-6454(99)00336-5.
- [36] L. Onsager, Reciprocal relations in irreversible processes. I., *Physical review* 37 (4) (1931) 405. doi:https://doi.org/10.1103/PhysRev.37.405.
- [37] S. De Groot, P. Mazur, Extension of Onsager’s theory of reciprocal relations. I., *Physical Review* 94 (2) (1954) 218. doi:https://doi.org/10.1103/PhysRev.94.218.
- [38] S. R. De Groot, P. Mazur, *Non-equilibrium thermodynamics*, Dover, New York, 1984.
- [39] J. Svoboda, F. Fischer, P. Fratzl, A. Kroupa, Diffusion in multi-component systems with no or dense sources and sinks for vacancies, *Acta Materialia* 50 (6) (2002) 1369–1381. doi:10.1016/S1359-6454(01)00443-8.
- [40] Y. Mishin, J. A. Warren, R. F. Sekerka, W. J. Boettinger, Irreversible thermodynamics of creep in crystalline solids, *Physical Review B* 88 (18) (2013) 184303. doi:10.1103/PhysRevB.88.184303.
- [41] Y. Mishin, G. B. McFadden, R. F. Sekerka, W. J. Boettinger, Sharp interface model of creep deformation in crystalline solids, *Physical Review B* 92 (6) (2015) 064113. doi:10.1103/PhysRevB.92.064113.
- [42] R. Ramanathan, P. W. Voorhees, Departures from local interfacial equilibrium during metal oxidation, *Physical Review Materials* 4 (11) (2020) 113401. doi:10.1103/PhysRevMaterials.4.113401.
- [43] S. Chatterjee, N. Moelans, A grand-potential based phase-field approach for simulating growth of intermetallic phases in multicomponent alloy systems, *Acta Materialia* 206 (2021) 116630. doi:10.1016/j.actamat.2021.116630.
- [44] J. Andersson, J. Ågren, Models for numerical treatment of multicomponent diffusion in simple phases, *Journal of Applied Physics* 72 (4) (1992) 1350–1355. doi:10.1063/1.351745.
- [45] J. Ågren, Diffusion in phases with several components and sublattices, *Journal of Physics and Chemistry of Solids* 43 (5) (1982) 421–430. doi:10.1016/0022-3697(82)90152-4.
- [46] K. Wang, F. Liu, Applications of irreversible thermodynamics to rapid solidification of multicomponent alloys, *Materials*

- Science and Technology 31 (13) (2015) 1642–1648. doi:10.1179/1743284715Y.0000000087.
- [47] E. T. Swartz, R. O. Pohl, Thermal boundary resistance, *Reviews of Modern Physics* 61 (3) (1989) 605–668. doi:10.1103/RevModPhys.61.605.
- [48] J. S. Langer, R. F. Sekerka, Theory of departure from local equilibrium at the interface of a two-phase diffusion couple, *Acta Metallurgica* 23 (10) (1975) 1225–1237. doi:10.1016/0001-6160(75)90041-3.
- [49] S. L. Sobolev, Effects of local non-equilibrium solute diffusion on rapid solidification of alloys, *Physica Status Solidi (a)* 156 (2) (1996) 293–303. doi:10.1002/pssa.2211560208.
- [50] S. L. Sobolev, Rapid solidification under local nonequilibrium conditions, *Physical Review E* 55 (6) (1997) 6845–6854. doi:10.1103/PhysRevE.55.6845.
- [51] H. Wang, P. Galenko, X. Zhang, W. Kuang, F. Liu, D. Herlach, Phase-field modeling of an abrupt disappearance of solute drag in rapid solidification, *Acta Materialia* 90 (2015) 282–291. doi:10.1016/j.actamat.2015.02.021.
- [52] R. S. Hixson, M. A. Winkler, M. L. Hodgdon, Sound speed and thermophysical properties of liquid iron and nickel, *Physical Review B* 42 (10) (1990) 6485–6491. doi:10.1103/PhysRevB.42.6485.
- [53] P. Galenko, S. Sobolev, Local nonequilibrium effect on undercooling in rapid solidification of alloys, *Physical Review E* 55 (1) (1997) 343–352. doi:10.1103/PhysRevE.55.343.
- [54] H. Ramalingam, M. Asta, A. van de Walle, J. Hoyt, Atomic-scale simulation study of equilibrium solute adsorption at alloy solid-liquid interfaces, *Interface Science* 10 (2) (2002) 149–158. doi:10.1023/A:1015889313170.
- [55] E. Antillon, C. A. Hareland, P. W. Voorhees, *Untitled manuscript*, unpublished (2022).
- [56] W. J. Boettinger, S. R. Coriell, Microstructure formation in rapidly solidified alloys, in: P. R. Sahm, H. Jones, C. M. Adam (Eds.), *Science and Technology of the Undercooled Melt: Rapid Solidification Materials and Technologies*, Springer Netherlands, Dordrecht, 1986, pp. 81–109. doi:10.1007/978-94-009-4456-5_5.
- [57] W. Kurz, D. Fisher, *Fundamentals of Solidification*, 3rd Edition, Trans Tech Publications, Aedermannsdorf, Switzerland, 1992.
- [58] R. Trivedi, W. Kurz, Dendritic growth, *International Materials Reviews* 39 (2) (1994) 49–74. doi:https://doi.org/10.1179/imr.1994.39.2.49.
- [59] H. Biloni, W. J. Boettinger, Chapter 8 - Solidification, in: R. W. Cahn, P. Haasen (Eds.), *Physical Metallurgy* (Fourth Edition), North-Holland, Oxford, 1996, pp. 669–842. doi:10.1016/B978-044489875-3/50013-2.
- [60] J. L. Murray, Calculations of stable and metastable equilibrium diagrams of the Ag-Cu and Cd-Zn systems, *Metallurgical Transactions A* 15 (2) (1984) 261–268. doi:10.1007/BF02645110.
- [61] J.-O. Andersson, T. Helander, L. Höglund, P. Shi, B. Sundman, Thermo-Calc & DICTRA, computational tools for materials science, *Calphad* 26 (2) (2002) 273–312.
- [62] Thermo-Calc, Thermo-Calc Software AB, Sweden (2021). URL <https://thermocalc.com>
- [63] W. H. Press, S. A. Teukolsky, W. T. Vetterling, B. P. Flannery, *Numerical recipes 3rd edition: The art of scientific computing*, Cambridge University Press, 2007.
- [64] Thermo-Calc Software, Sweden, Thermo-Calc Documentation Set, version 2022a (2022).
- [65] M. Buchmann, M. Rettenmayr, Rapid solidification theory revisited – A consistent model based on a sharp interface, *Scripta Materialia* 57 (2) (2007) 169–172. doi:10.1016/j.scriptamat.2007.02.039.
- [66] K. Reuther, S. Hubig, I. Steinbach, M. Rettenmayr, Solute trapping in non-equilibrium solidification: A comparative model study, *Materialia* 6 (2019) 100256. doi:10.1016/j.mtl.2019.100256.
- [67] P. Galenko, Solute trapping and diffusionless solidification in a binary system, *Physical Review E* 76 (3) (2007) 031606. doi:10.1103/PhysRevE.76.031606.
- [68] S. L. Sobolev, Local non-equilibrium diffusion model for solute trapping during rapid solidification, *Acta Materialia* 60 (6) (2012) 2711–2718. doi:10.1016/j.actamat.2012.01.036.
- [69] P. Galenko, Extended thermodynamical analysis of a motion of the solid-liquid interface in a rapidly solidifying alloy, *Physical Review B* 65 (14) (2002) 144103. doi:10.1103/PhysRevB.65.144103.
- [70] P. Galenko, Rapid advancing of the solid-liquid interface in undercooled alloys, *Materials Science and Engineering: A* 375–377 (2004) 493–497. doi:10.1016/j.msea.2003.10.013.
- [71] M. Hillert, Solute drag in grain boundary migration and phase transformations, *Acta Materialia* 52 (18) (2004) 5289–5293. doi:10.1016/j.actamat.2004.07.032.

- [72] M. Buchmann, M. Rettenmayr, Non-equilibrium transients during solidification – A numerical study, *Scripta Materialia* 58 (2) (2008) 106–109. doi:10.1016/j.scriptamat.2007.09.022.
- [73] E. Gamsjäger, M. Rettenmayr, The kinetics of diffusive phase transformations in the light of trans-interface diffusion, *Philosophical Magazine* 95 (26) (2015) 2851–2865. doi:10.1080/14786435.2015.1078514.
- [74] K. Wang, H. Wang, F. Liu, H. Zhai, Effect of thermodynamic interactions on the rapid solidification kinetics of Ni-Cu-Co alloys, *Metallurgical Research & Technology* 111 (5) (2014) 321–328. doi:10.1051/metal/2014013.
- [75] J. W. Cahn, The impurity-drag effect in grain boundary motion, *Acta Metallurgica* 10 (9) (1962) 789–798. doi:10.1016/0001-6160(62)90092-5.
- [76] M. Alkayyali, F. Abdeljawad, Grain boundary solute drag model in regular solution alloys, *Physical Review Letters* 127 (17) (2021) 175503. doi:10.1103/PhysRevLett.127.175503.
- [77] J. Kittl, P. Sanders, M. Aziz, D. Brunco, M. Thompson, Complete experimental test of kinetic models for rapid alloy solidification, *Acta Materialia* 48 (20) (2000) 4797–4811. doi:10.1016/S1359-6454(00)00276-7.
- [78] H. S. Zurob, D. Panahi, C. R. Hutchinson, Y. Brechet, G. R. Purdy, Self-Consistent Model for Planar Ferrite Growth in Fe-C-X Alloys, *Metallurgical and Materials Transactions A* 44 (8) (2013) 3456–3471. doi:10.1007/s11661-012-1479-8.
- [79] M. Gouné, F. Danoix, J. Ågren, Y. Bréchet, C. R. Hutchinson, M. Militzer, G. Purdy, S. van der Zwaag, H. Zurob, Overview of the current issues in austenite to ferrite transformation and the role of migrating interfaces therein for low alloyed steels, *Materials Science and Engineering: R: Reports* 92 (2015) 1–38. doi:10.1016/j.mser.2015.03.001.